

Review

Review of Control Techniques in Microinverters

Diego Rojas ¹, Javier Muñoz ^{1,*}, Marco Rivera ¹ and Jaime Rohten ²

¹ Engineering Systems Doctoral Program, Faculty of Engineering, University of Talca, 3340000 Curicó, Chile; dnprojas@gmail.com (D.R.); marcoriv@utalca.cl (M.R.)

² Department of Electrical and Electronic Engineering, Universidad Del Bío-Bío, Avenida Collao 1202, 4051381 Concepción, Chile; jrohten@ubiobio.cl

* Correspondence: jamunoz@utalca.cl

Abstract: The use of renewable energies sources is taking great importance due to the high demand for electricity and the decrease in the use of fossil fuels worldwide. In this context, electricity generation through photovoltaic panels is gaining a lot of interest due to the reduction in installation costs and the rapid advance of the development of new technologies. To minimize or reduce the negative impact of partial shading or mismatches of photovoltaic panels, many researchers have proposed four configurations that depend on the power ranges and the application. The microinverter is a promising solution in photovoltaic systems, due to its high efficiency of Maximum Power Point Tracking and high flexibility. However, there are several challenges to improve microinverter's reliability and conversion efficiency that depend on the proper control design and the power converter design. This paper presents a review of different control strategies in microinverters for different applications. The control strategies are described and compared based on stability, dynamic response, topologies, and control objectives. One of the most important results showed that there is little research regarding the stability and robustness analysis of the reviewed control strategies.

Keywords: control strategies; DC-DC converter; DC-AC converter; microinverter; maximum power point tracking; photovoltaic



Citation: Rojas, D.; Muñoz, J.; Rivera, M.; Rohten, J.A. Review of Control Techniques in Microinverters. *Sensors* **2021**, *21*, 6486. <https://doi.org/10.3390/s21196486>

Academic Editors: J. C. Hernandez, Carlos R. Baier and Pat Wheeler

Received: 26 August 2021

Accepted: 15 September 2021

Published: 28 September 2021

Publisher's Note: MDPI stays neutral with regard to jurisdictional claims in published maps and institutional affiliations.



Copyright: © 2021 by the authors. Licensee MDPI, Basel, Switzerland. This article is an open access article distributed under the terms and conditions of the Creative Commons Attribution (CC BY) license (<https://creativecommons.org/licenses/by/4.0/>).

1. Introduction

Electricity generation systems through photovoltaic panels are becoming increasingly important within renewable energies sources, since the costs associated with photovoltaic panels have decreased and the efficiency of power converters have increased [1]. Due to environmental policies and the growth in electricity demand, the use of photovoltaic panels has grown worldwide, today having a total installed capacity of 623 GW approximately [2]. However, when implementing or selecting an electrical generation system, high robustness should be considered in the face of voltage variations, current or power outage, high reliability (appropriate waveforms for both voltage and current and supply of electrical energy in all moment), and an adequate power capacity for the design requirements, in order to obtain a good electrical production performance. These systems generate many transient, due to the variation in the solar radiation, and therefore a non-continuous supply, leading to power quality issues [3,4]. A significant part of the photovoltaic installations are the power conditioning system, also known as power converters, which transform the electrical power, generated by the photovoltaic panels, into a signal suitable for use. In order to mitigate these problems, or reduce the negative effects, different configurations have been proposed, such as the string, multistring, central, and ac module, where the main differences are given by the power range. For example, a string configuration operates between 1 kW and 10 kW (residential application), a multistring configuration operates between 10 kW and 30 kW (residential or commercial application), a central configuration operates from 30 kW (large-scale photovoltaic plants), and a ac module configuration or microinverter operates at a maximum of 500 W (small-scale systems) [5]. Moreover, they

are also differentiated by the series and parallel combination of the photovoltaic panels and their respective connection to the power converters.

The central configuration has arrived to the market with the greatest impact, having a market-share of almost 95%, due to its high efficiency (close to 98%) and the high demand for electricity generation [6]. On the other hand, a microinverter is a configuration which allows for the integration of photovoltaic solar energy, where each photovoltaic module contains its own converter. They are also known as ac modules or integrated module inverters, because they are small and operate in a low power range [1]. The advantages of this configuration are high Maximum Power Point Tracking (MPPT) efficiency, ease of installation, flexibility, being modular, better amortization of the initial investment [7], ease of monitoring and detecting faults [1], applications in small power, and it can be installed in complex structures with different orientations and it is not necessary to incorporate bypass diode [7].

However, up to now the microinverter's configuration has a low market entry, having a market-share of less than 10%, low operating power ranges, and low reliability. Other shortcomings are low conversion efficiency (up to 96.5% [1,6]), higher cost per watt, and in the absence of boost converter it requires a bulky power transform and it requires a high boost to pump up the voltage to the grid level.

Due to the rapid development of new power semiconductors, microinverters are an emerging and promising solution to mitigate the partial shading and dirt-effect problems. Thanks to the recent advances, it will be possible to increase the ranges of power and conversion efficiency. In addition, to ensure a safe, reliable, and efficient energy conversion from photovoltaic generation systems, it is very important to consider the adequate design of the control of the power converters, as well as the topology configuration. Hence, control strategies are important to regulate the different voltage and current levels for the requirements of different applications, with the aim of increasing the reliability of the microinverter. Therefore, this paper will be focused on different types of control strategies applied in microinverters for a range of purposes.

2. Microinverter

Microinverters can be classified into four categories [8,9], such as: one-stage topology without galvanic isolation; two-stage topology without galvanic isolation; one-stage topology with galvanic isolation; and two-stage topology with galvanic isolation.

Figure 1 shows the configuration of each category. In a two-stage topology, it consists of a dc-dc converter that performs the MPPT, and the dc-ac converter has the responsibility of controlling the dc-link and the control of the grid current or properly controlling the output voltage in island mode. In terms of control, the two-stage topology is simple, and the dc-dc converter also extends the operation of the photovoltaic system, leading to a decrease in overall efficiency [6]. One-stage topologies are introduced to reduce power losses and reduce the total system volume [6].

On the other hand, microinverters can also be classified by the incorporation of galvanic isolation depending on the electrical policies of each country, as well as the needs of photovoltaic installation. The incorporation of a transformer allows for the isolation of the photovoltaic generation stage and the consumption stage or the grid, with the aim that if panels fail, it does not have direct impact on the grid or on local loads. In addition, the transformer allows reaching high levels of voltage, which is required for integration to the grid; however, it leads to a reduction in efficiency reduction and an increase in the microinverter's volume [6,8,10].

However, there are certain challenges in positioning microinverters as an attractive alternative on the market [6,8], such as: to increase reliability and lifespan due to sensitivity to the temperature of the electrolytic capacitors; to increase conversion efficiency considering cutting-edge semiconductors and development of new high-gain converter topologies; and to increase the functionality of the microinverters, adding some other tasks such as reactive power support and power supply at all times.

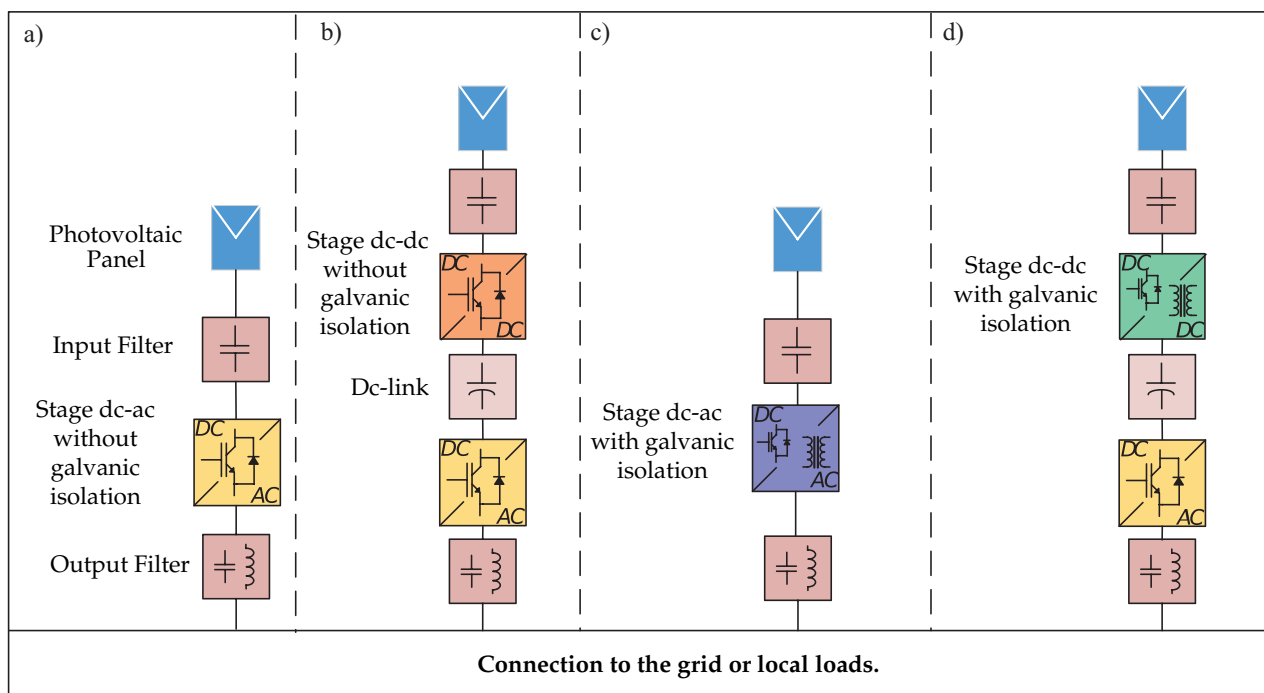


Figure 1. Classification of microinverters. (a) One-stage topology without galvanic isolation. (b) Two-stage topology with galvanic isolation. (c) One-stage topology with galvanic isolation. (d) Two-stage topology with galvanic isolation.

Design Challenges

Despite having several advantages, in the market they are not the device that users buy the most due to low power ranges, low reliability, and low conversion efficiency compared to the other configurations [6]. Other disadvantages are that they have a single function, aimed to make the conversion of electrical energy necessary for their use or inject into the grid. Microinverters are usually equipped with bulky, low-reliability capacitors, which have a high rate of failure [7]. On the other hand, because solar energy is intermittent, a storage system with high capacity and a fast charging/discharging is required. One of the possible solutions to improve reliability is the incorporation of a hybrid storage (supercapacitor and battery) with the aim of increasing power density and energy density. Moreover, the cost of rechargeable energy storage has decreased drastically in recent years due to technological advances due to higher penetration of distributed Renewable Energy Sources. Additionally, if this battery/ultracapacitor hybrid energy storage system is embedded in the PV micro-inverters, the problem of reliability that electrolytic-capacitor-based micro-inverters have can be overcome, together with the filtering of the power ripple, and it will allow an additional ancillary service as backup for the power grid acting as a distributed Uninterruptible Power Supply, providing a distributed inertia to the utility grid.

On the other hand, the proposed solution to increase power capacities, improve efficiency, and reduce the size of the microinverter is the implementation of semiconductors based on Gallium-Nitride and Silicon-Carbide since they are characterized by being of high efficiency, high power density, high frequency operation, and they decrease the size of the converter [11]. As these materials allow much higher switching speeds, it implies smaller passive components, increasing thus the power density of micro-inverters but also taking into account that the circuit parasitics and the associated electromagnetic interference may be reduced to unprecedentedly low levels, demanding new approaches of fully integrated assemblies comprising power devices, gate drives, filters, and control functions.

3. Control Strategies

This section presents a review of control strategies applied to microinverters and it is organized depending on the control application: grid connected, islanding mode (off-grid),

reactive power compensation, photovoltaic system including energy storage, and multiple operation mode or multiple functions.

3.1. Grid Connected

The reference [12] presents a hybrid hysteresis current control $G_{HCC}(s)$ and a low-frequency harmonic mitigation strategy based on a PR (Proportional-Resonant) control $G_{PR}(s)$. The microinverter's topology is a full-bridge inverter for the PV system (Figure 2). The main objective is to reduce the switching losses and achieve an optimized grid current. Figure 3 shows the proposed control strategy. Due to a wide hysteresis band for smooth switching, low output inductance, and digital controller sampling time, the error between the reference current $i^*(t)$ and the average inductor output current still results from many low frequency harmonics, so the current grid $i_g(t)$ must be sensed and compared to a reference. The low frequency error can be mitigated by the PR controller and the power quality of the electrical grid could be improved.

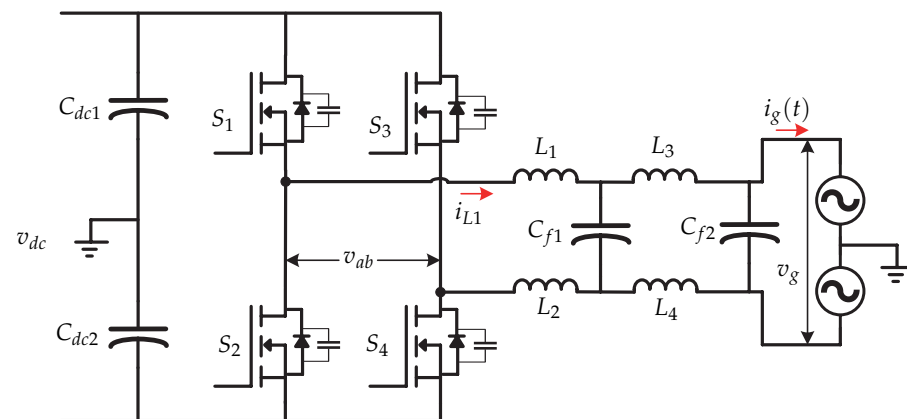


Figure 2. Microinverter's topology proposed in [12].

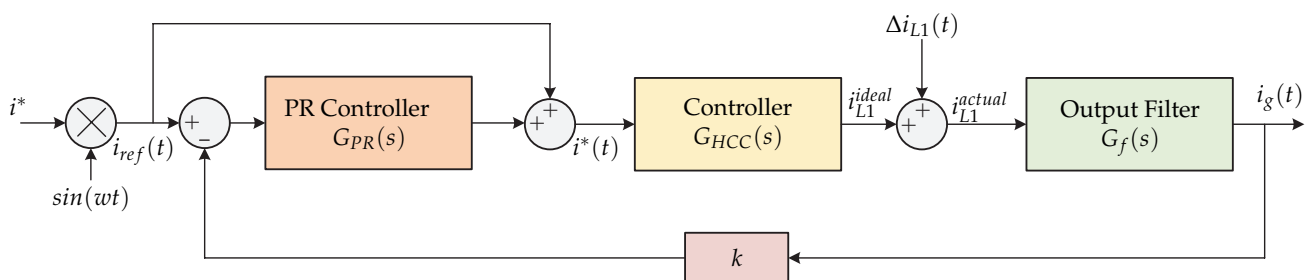


Figure 3. Control strategy proposed in [12].

In [13,14] a two-stage microinverter consisting of a boost-half-bridge converter connected to an full-bridge inverter is presented (Figure 4). The control strategy is presented in Figure 5. The dc-dc converter is in charge of the maximum power point tracking and generates the voltage reference v_{pv}^* , which is compared with the voltage of the photovoltaic panel v_{pv} . The voltage error is minimized by a Proportional-Integral controller (PI), and the result is summed up to the panel photovoltaic voltage reference and compared with the derivative of the panel voltage. The result is the modulating pattern, which is compared to a triangular carrier signal that generates the switching signal of the dc-dc converter. In the dc-ac stage there is a double control loop, where the external voltage loop is handled by a PI controller that generates the grid peak current reference. Then, it is compared with the norm of the inverter current $|i_{inv}|_{ff}$ and then the result is multiplied by a sinusoidal signal $\sin(\theta_g)$ whose angle is obtained from a Phase Locked Loop (PLL). This inverter current reference i_{inv}^* is compared with the sensed inverter current i_{inv} whose result is minimized

by a repetitive controller (Plug-in RC) to generate the switching signals of the full-bridge inverter. To achieve fast dynamic responses in both grid current as well as dc-link voltage, a feed-forward current reference is added to the control strategy.

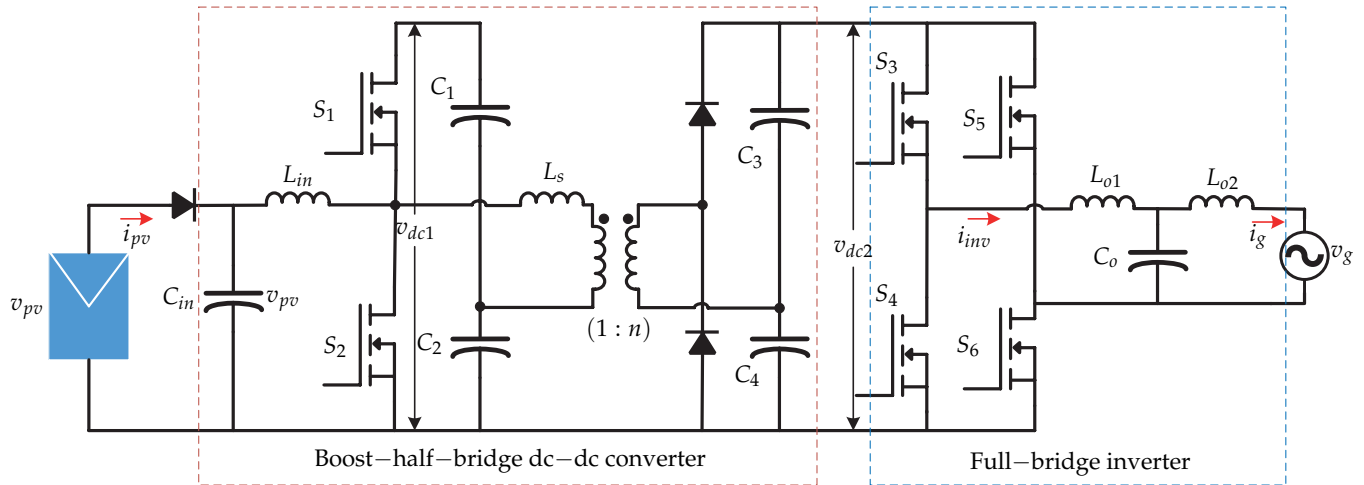


Figure 4. Microinverter's topology proposed in [13,14].

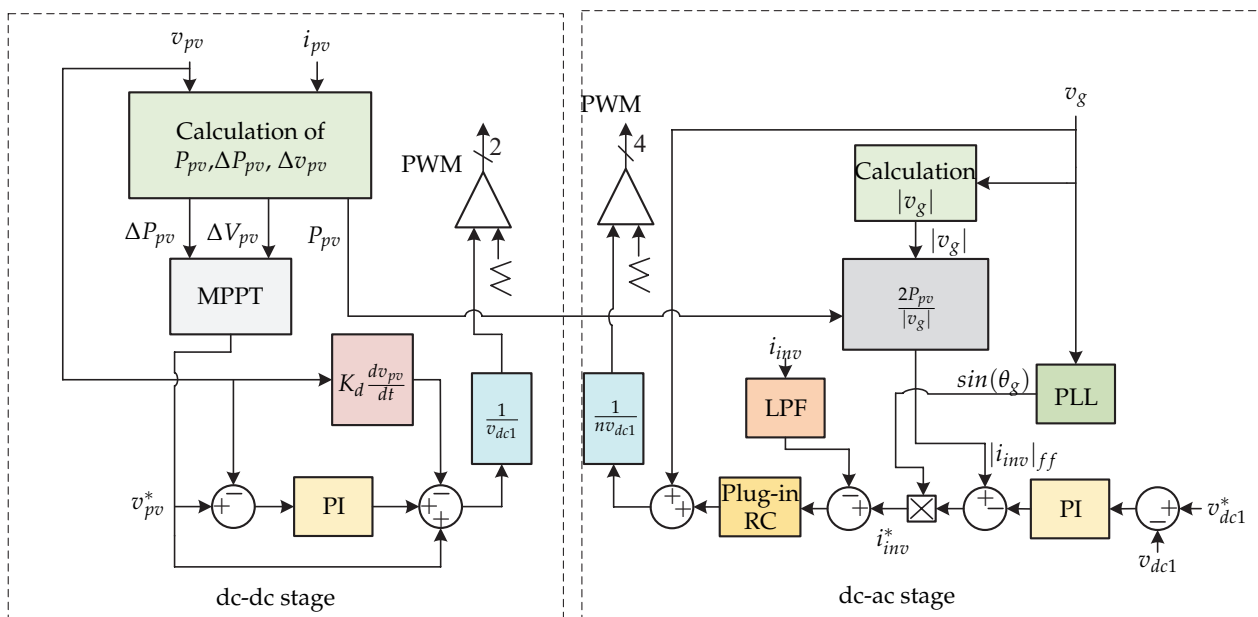


Figure 5. Control strategy proposed in [13,14].

The references [15,16] present a dual-stage microinverter, where in the first stage is an LLC resonant dc-dc converter and in the second stage a three-phase zero-voltage-switching (ZVS) dc-ac converter (Figure 6). The variables to be controlled in the microinverter are the inductor currents (i_{L2}^a , i_{L2}^b and i_{L2}^c) used as a filter, the dc-link voltage v_{dc} and the currents injected into the grid (i^a , i^b , i^c). Figure 7 presents the control strategy. The objective of the dc-dc converter is to track the maximum power point by means of an MPPT algorithm, whose function is to define the switching signal f_s based on the power of the photovoltaic panel. In the dc-ac stage, the proposed control strategy is that of a triple loop controller. In order to balance the power of the photovoltaic panel and the power of the electrical network, it is necessary to have a constant dc-link voltage. This is done by comparing the dc-link voltage v_{dc} with a reference v_{dc}^* and the result is controlled by a dc-link controller that generates the current reference in the d -frame and is compared with the current i_d

obtained by the dq transformation. The result is controlled by a PI controller that generates the voltage reference in the d -frame v_d^* which is sum to the grid voltage. The Q control is not explained in [15] because reference current in q -frame is considered zero. On the other hand, the reference current i_q^* compared with the grid current in the q -frame is controlled by the mean of a PI controller to generate the reference grid voltage in the q -frame v_q^* which is which is the reference for the sensed grid voltage v_q . Then, the reference three-phase current (I_a^* , I_b^* and I_c^*), and then it is compared with the inductance currents ($i_{L1}^a, i_{L1}^b, i_{L1}^c$) in order to generate the switching sequence.

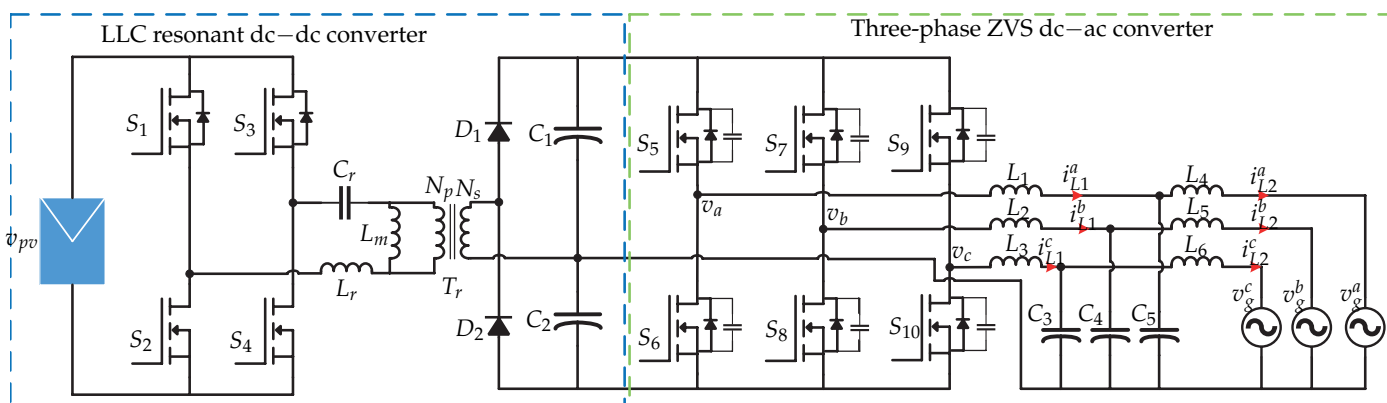


Figure 6. Microinverter’s topology proposed in [15].

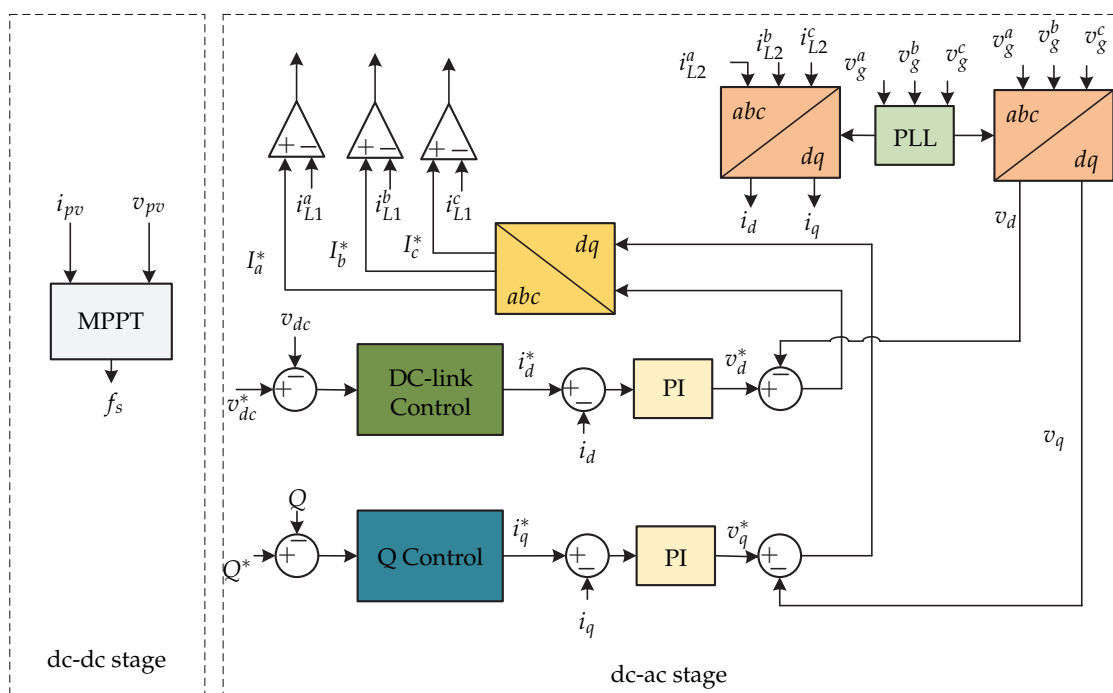


Figure 7. Control strategy proposed in [15–17].

In [18] a microinverter without galvanic isolation is presented and it consists of a topology derived from a non-inverted Cuk converter connected to an inverted Cuk converter (Figure 8). The proposed control strategy is presented in Figure 9. The control strategy consists of an MPPT algorithm that generates the reference voltage v_{pv}^* that is compared with the voltage of the instantaneous photovoltaic panel v_{pv} . The result is processed by a PI voltage controller that generates the current for the photovoltaic panel at the maximum power point i_{mpp} . This signal is multiplied by the $\sin\theta$ provided by a PLL to

synchronize the signal with the grid voltage, obtaining the inductor current reference i_{L2}^* . This signal is compared with the sensed inductor current i_{L2} and is processed by a PR type current controller to generate the modulator m_a . This modulating signal is necessary to generate the switching sequence by means of a SPWM.

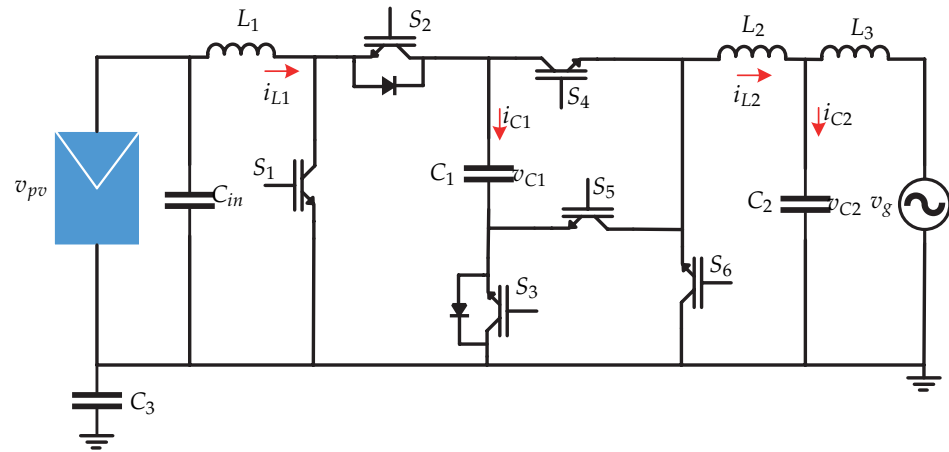


Figure 8. Microinverter's topology proposed in [18].

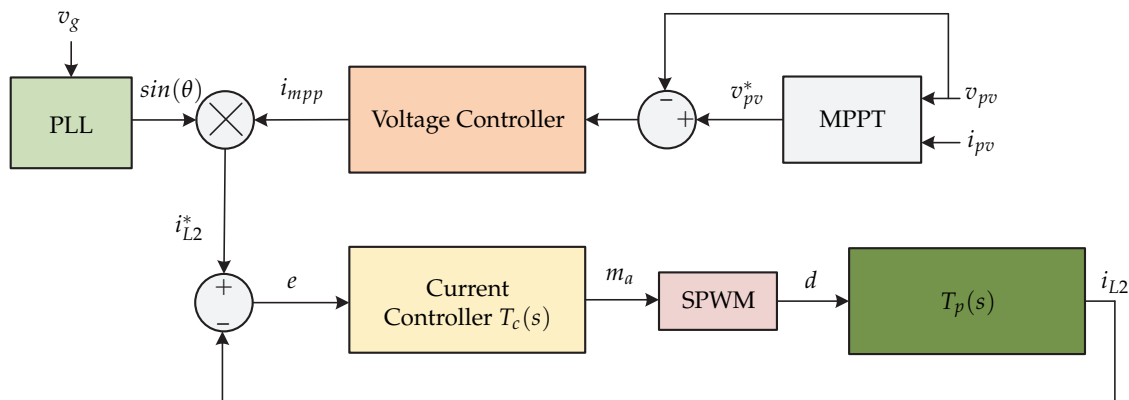


Figure 9. Control strategy proposed in [18].

In [19,20] a current sensorless control strategy is proposed for a dual stage microinverter. It consists of a flyback dc-dc converter connected to a voltage source inverter for the current injection to the electrical grid (Figure 10). The advantage of this proposal is the cost derived from current sensors by minimizing and reducing measurement noise introduced to the control algorithm. The control strategy is presented in Figure 11 and consists of an observer that estimates the inductance values to calculate the inductor current based on the comparison between the results of two calculations of the current. The state observer estimates the value of the magnetizing current $\hat{i}_{L,pri}$ and the current of the photovoltaic panel \hat{i}_{pv} . Then, the MPPT (Perturb and Observe) algorithm generates the photovoltaic panel voltage v_{pv}^* reference which is compared to the sensed photovoltaic panel voltage v_{pv} . The result is processed by a PI controller that generates the maximum permissible magnetizing current $i_{L,pri}^{max}$ and is multiplied by the voltage of the synchronized network to generate the peak magnetization current $i_{L,pri}^{pk}$. Finally, a peak current control (PCM) is developed to generate the switching signal S_p that depends on the peak magnetization current and the estimated magnetization current. It is worth mentioning that the proposed work only presents the control strategy for the dc-dc stage and an open loop for the inverter, leaving the control strategy for the dc-ac stage as future work.

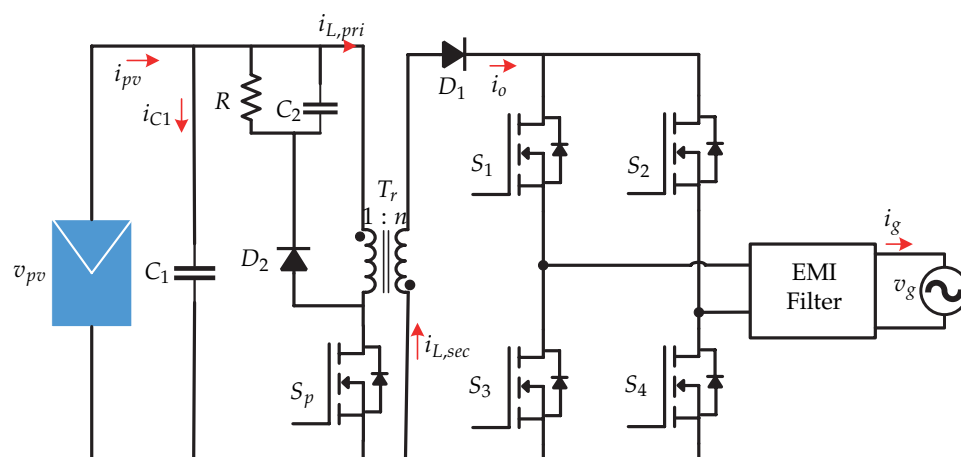


Figure 10. Microinverter's topology proposed in [19,20].

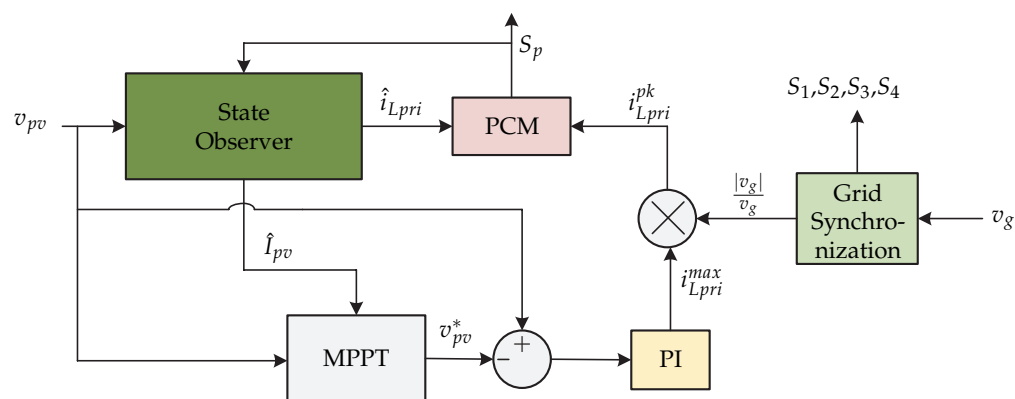


Figure 11. Control strategy proposed in [19,20].

In [21–24] a microinverter (Figure 12) based on a direct digital synthesis technique is presented for operation in grid-connected mode. This technique provides flexibility in implementation of various controls such as MPPT, PLL, anti-island, and low-voltage ride-through (LVRT). The control strategy is presented in Figure 13 and consists of the MPPT algorithm based on the constant voltage method (CVT) for the dc-dc stage, which requires sensing the voltage and current of the photovoltaic panel (v_{pv} y i_{pv}). The MPPT algorithm generates the voltage at the maximum power point V_{mpp} and it is compared with a reference voltage v_{pv}^* and the error is processed by a PI controller that generates the d frame current (i_d). On the other hand, the grid voltage v_g and the grid current i_s are sensed to generate the currents and voltages in dq frame that are used by a dq power estimator. The output of the estimator is the Q reactive power which is compared with the reference reactive power Q^* . The error is processed by a PI controller that generates the current in q frame (i_q). Then, the dq frame currents are transformed to the $\alpha\beta$ frame. In summary, the d component regulates the output voltage v_o and the q component determines the reactive power to be injected into the grid.

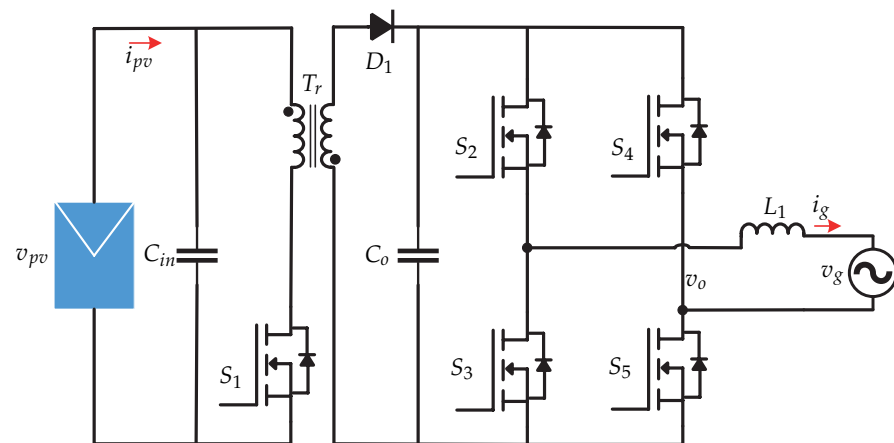


Figure 12. Microinverter's topology proposed in [21–24].

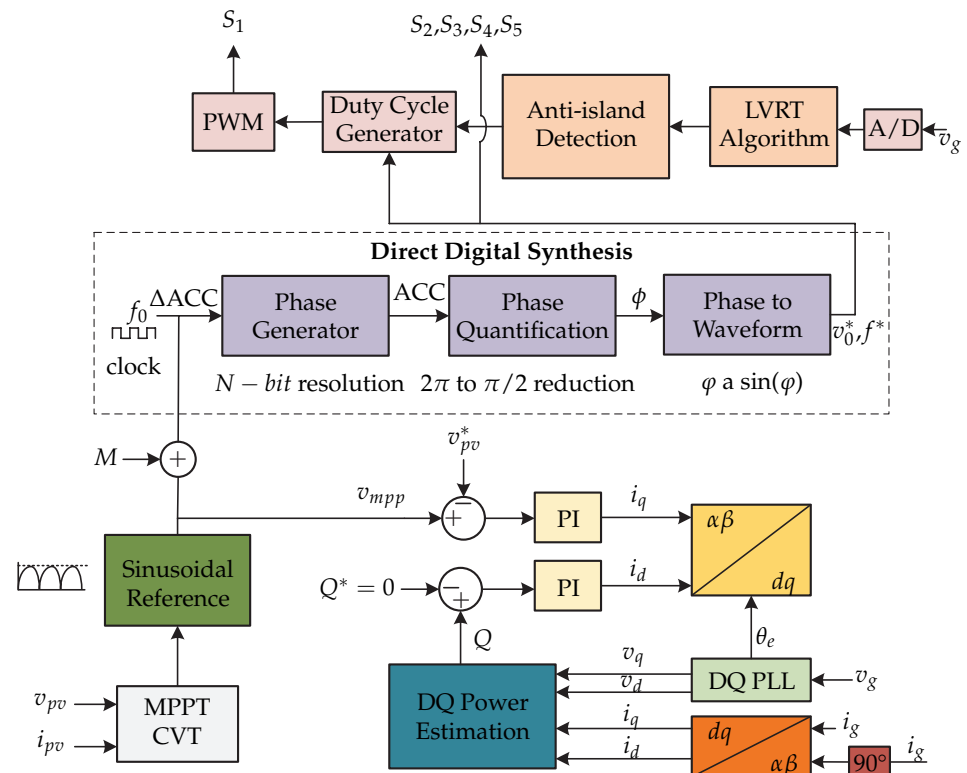


Figure 13. Control strategy proposed in [21–24].

In [25] a microinverter consisting of two stages is presented. The dc-dc stage consists of a flyback converter with an *active-clamp* circuit in the primary part of the transformer and a *series resonant voltage doubler* in the secondary part of the transformer (Figure 14). The *active-clamp* circuit allows for the operation of the switches in zero-voltage switching by limiting the voltage across the active power semiconductors and therefore reducing the losses. The control strategy is presented in Figure 15 which consists of the MPPT algorithm that generates the amplitude of the grid current reference I_g^* . This is multiplied by the signal obtained from the PLL in order to obtain the reference grid current i_g^* . Then this signal is compared to the grid current $|i_g|$ to generate the variation of the duty cycle ΔD by means of a proportional controller k_{pg} . The term $|v_g|/v_{dc}$ is the product of the applied feedback linearization, to decouple the variation of the duty cycle with rated duty cycle D_{nom} , in order to make the relationship between of the variation of the grid current Δi_g and ΔD first order and linear. Furthermore, the voltage regulation is performed on the dc-link voltage v_{dc} by means of a voltage controller. The signal generated by the voltage

controller and the sum of the duty cycle variation and the rated duty cycle generate the switching signals for the dc-dc converter and the dc-ac converter (S_1, S_2, S_3, S_4).

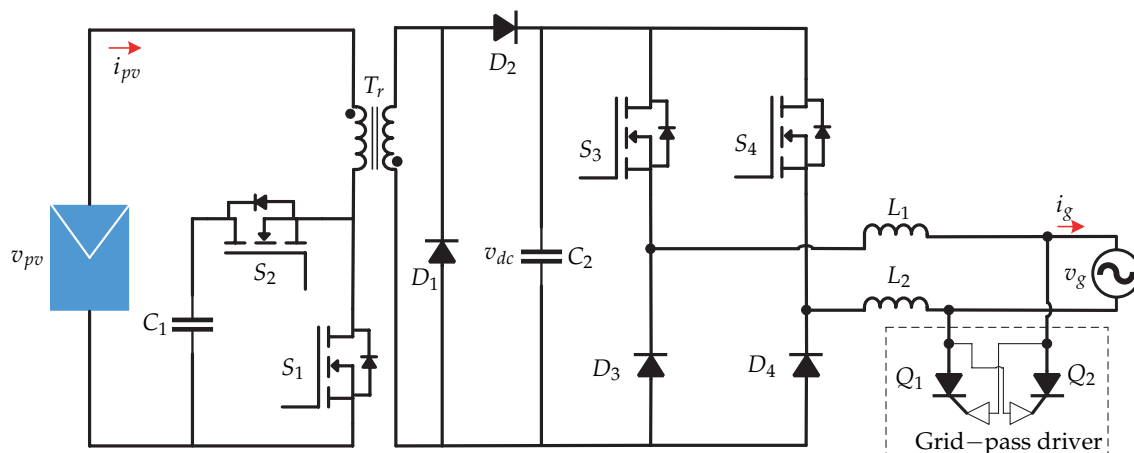


Figure 14. Microinverter's topology proposed in [25].

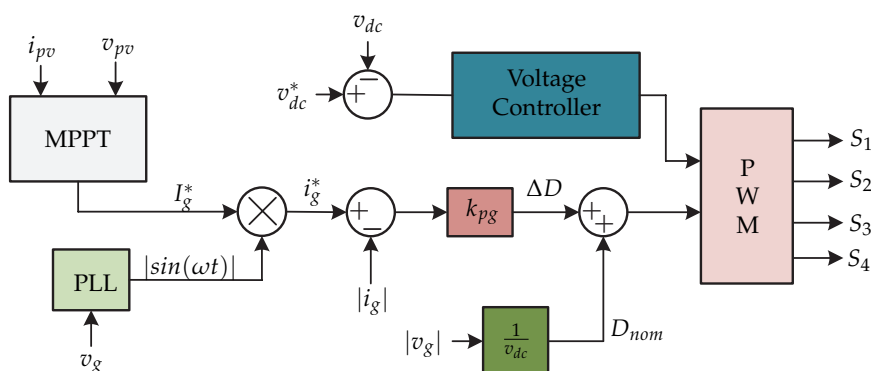


Figure 15. Control strategy proposed in [25].

In [26] a single stage dc-ac microinverter is presented consisting of a coupled-inductor double-boost inverter (Figure 16). The main characteristics are: simple structure, generation of an ac output in magnitude greater than the dc signal, small volume, and high efficiency. The control strategy is presented in Figure 17. The control consists of an MPPT P and O algorithm where the reference voltage of the photovoltaic panel V_{pv}^* is obtained and it is compared with the photovoltaic panel voltage v_{pv} , whose error is processed by a PI voltage control to generate the current amplitude I_m . The amplitude is multiplied by a sinusoidal signal, whose angle is obtained from a PLL for synchronization with the grid, obtaining the reference of the output current i_o^* . The reference is compared with the output current i_o and enters a current controller proposed in [26] and allows canceling the dc components of the inductor current, as well as canceling some poles and zeros of the proposed converter model.

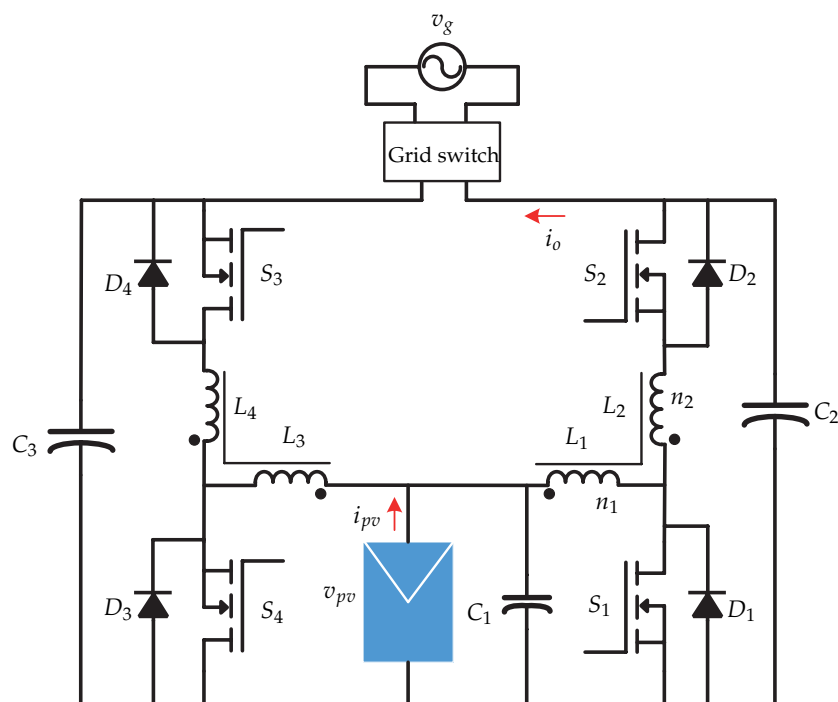


Figure 16. Microinverter’s topology proposed in [26].

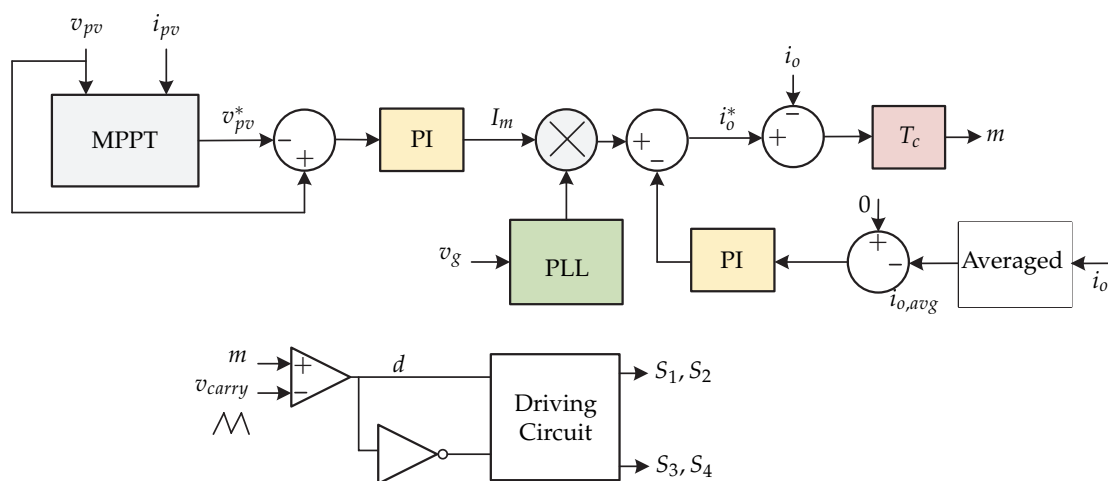


Figure 17. Control strategy proposed in [26].

In [27,28], the study of the dc-dc stage of a microinverter is presented, which is suitable for connecting it to a dc-ac stage and integrating it with the grid (Figure 18). A topology of a dual-mode rectifier (DMR) based series resonant dc-dc converter is proposed and its characteristics are: ability to operate in a wide variety of voltage inputs and high efficiency. The control strategy proposed for the dc-dc converter is presented in Figure 19 and its main characteristic is its variable dc-link voltage control, with the aim of reducing RMS (root mean square) currents, improving the efficiency of the microinverter. In addition, it is characterized by being a flexible control, since it has two modes of operation. For the case of the control of the MPPT, Mode 1 will be applied. The MPPT algorithm is executed and the voltage reference is compared with the voltage of the photovoltaic panel v_{pv} . Then the comparison result is processed by a PI control to get ϕ (inverter controls the dc-link). In Mode 2, the switch connects the dc source and disconnects the photovoltaic panel. Then, the variable control is executed which generates the reference voltage of the dc link v_o^* and is compared with the output voltage v_o . Finally, the result of the comparison is processed by

a PI control to obtain the value of ϕ . The switching sequence is generated by the modulator depending on the operating mode of the microinverter.

In [29] a control strategy for a two-stage topology is presented. In the first stage, it contains a flyback dc-dc converter and in the second stage it contains a full-bridge inverter (Figure 20). A microinverter with hybrid mode is presented and consists of a control strategy that allows the system to operate in both continuous and discontinuous mode. The advantages of operating in hybrid mode is the stress reduction faced by the primary and secondary part of the transformer [29]. The control strategy is presented in Figure 21. The proportional-resonant controller (PR controller) plus the harmonic compensator (HC) provide a high gain in the fundamental frequency and harmonics, in order to improve the performance of the discontinuous mode and the stability of the continuous mode of the flyback converter. In addition, the hybrid duty cycle obtained by means of the operating mode selector allows for the elimination of disturbances and reduces the load on the feedback controller.

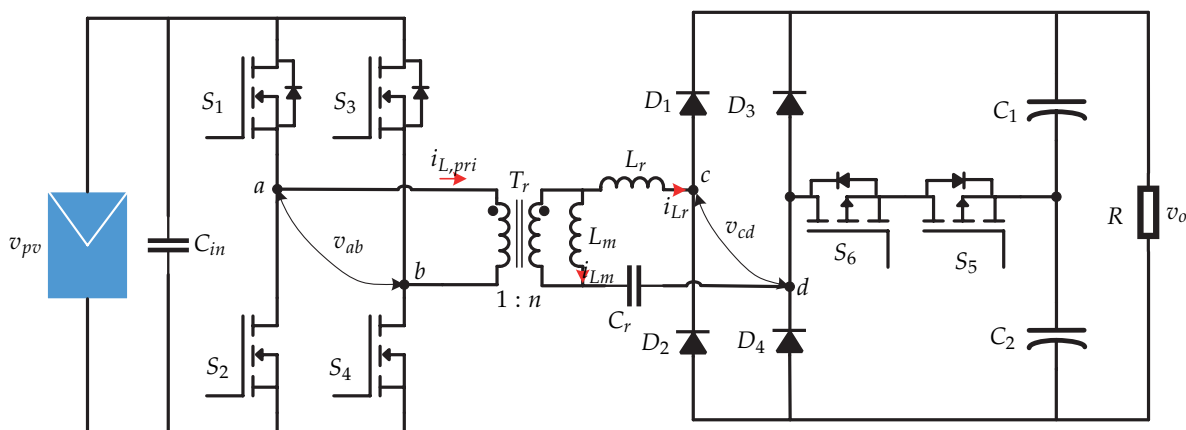


Figure 18. Microinverter’s topology proposed in [27,28].

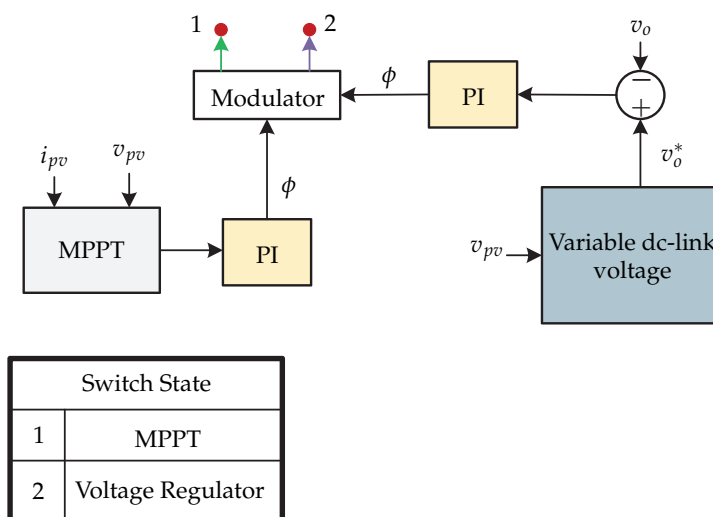


Figure 19. Control strategy proposed in [27].

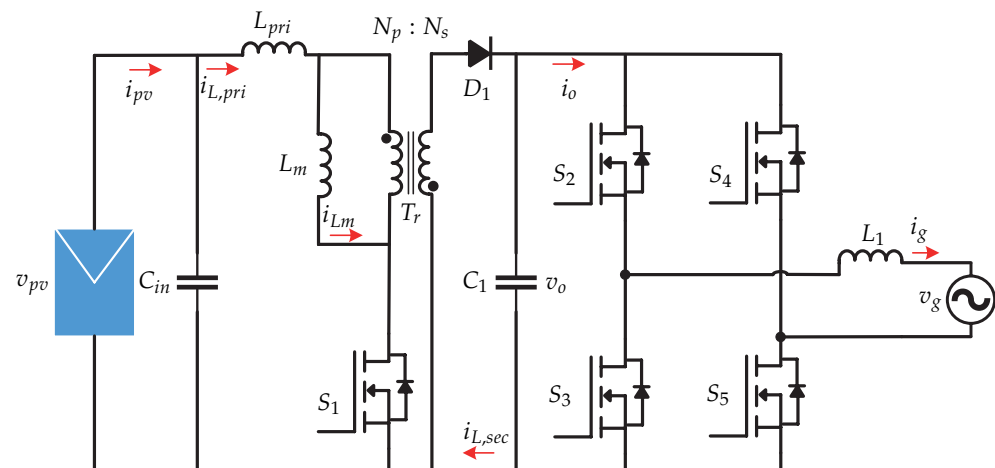


Figure 20. Microinverter's topology proposed in [29].

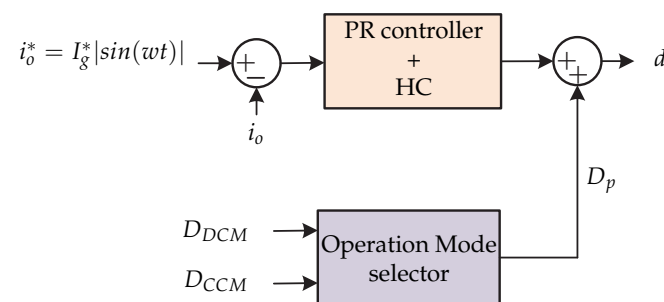


Figure 21. Control strategy proposed in [29].

Other control techniques are as follows:

- The paper [30] presents a Flyback PV microinverter with analog and digital controller. The analog control consists of a precision rectifier circuit, a pulse width modulation comparator, and zero-crossing detector. The aim of digital control is to obtain the Maximum Power Point from the Photovoltaic module.
- The paper [31] presents a differential boost microinverter. The control technique consists of a MPPT-loop control, a second loop that synchronizes the grid current to the grid voltage, and a three-loop differential peak current control.
- The paper [32] presents a two stage microinverter with LLC resonant converter. The control technique consists of a MPPT based a fixed-frequency model predictive control and a PI control.
- The paper [33] presents a microinverter based a cascaded boost converter with a full bridge. The control technique consists in two sliding control alternatives (input current mode and pseudo-oscillating mode).
- The paper [34] presents a microinverter based a interleaved flyback with an unfolding H-bridge inverter. The control technique consists in a novel sliding mode control current controller.
- The paper [35,36] presents a interleaved flyback with two stage unfolding cyclo-converter. The control strategy consists in a power-increment-aided incremental-conductance MPPT with constant-frequency variable-duty and a forward compensator.
- The paper [37] presents a dual-active-bridge (DAB) microinverter. The control strategy consists in simple closed-loop current control (PI controller).
- The paper [38] presents a switched capacitor buck-boost voltage source inverter (SC-BBVS). The control strategy consists in a PI controller for dc-link voltage regulation and proportional-resonant (PR) controller for injected current regulation.

- The paper [39] presents a two stage microinverter. This consists of a high step-up Z source dc-dc converter with a full-bridge inverter. The control technique is similar to [13] (Figure 4).
- The paper [40] presents a two stage microinverter and it consists of boost dc-dc converter with a single-phase full-bridge inverter. The control strategy consists in non-linear control techniques based of the non-linear average model of microinverter.
- The paper [41] presents a boost inverter and it consists of two boost dc-dc converters connected in differential mode to the grid. The control technique consists of a PI control for power reference and a flatness-based control. In [42], a flatness-based control is also presented.
- The paper [43,44] presents two microinverter topologies. First, a interleaved flyback dc-dc converter with unfolding inverter is presented and then a push-pull dc-dc converter with unfolding inverter. The proposed control strategy consists in a simple PR controller to generate a sinusoidal current reference waveform and PI controller to generate a power reference.
- The paper [45] presents a two-stage microinverter and it consists in a step-up isolation dc-dc converter with half-bridge inverter. The control technique consists in a PI controller in order to reduce the third harmonic. Moreover, it consists in a feedforward control.
- The paper [46] presents a full-bridge inverter for microinverter application. The control technique consists in a sliding mode control of the output current.
- The paper [47] presents a quadratic boost dc-dc converter with full-bridge inverter. The control technique consists in a sliding mode control for dc-link voltage and grid current regulation. The paper [48] presents the above topology, but the control strategy is based on PI controllers.
- The paper [49] presents a multi-level single phase microinverter and its control strategy consists in a model predictive control to reduce the steady state error of the grid-injected current. Another control technique used in this microinverter is the PI controller with PR controller proposed in [50].
- The paper [51] presents a single stage boost inverter, composed by a two bidirectional boost dc-dc converter. The control strategy consists in a finite control set model predictive control algorithm with predictions of the system variables.
- The paper [52] presents a full-bridge converter cascaded to a boost converter with other full-bridge converter. The control technique consists in a PI controller for dc-link voltage regulation and a PR controller used in the current control loop.
- The paper [53] presents a T-type microinverter in boundary conduction mode. The control technique consists in a hybrid control based on the proposed voltage equalization and adaptive reverse current control method.
- The paper [54] presents a high-gain Z-source boost converter with H-bridge inverter. The control strategy consists of a PI controller to regulate the dc-link voltage and hysteresis current control to regulate the grid current.
- The paper [55] presents a resonant microinverter and its control strategy consists of different PI controllers.
- The paper [56] presents a microinverter based in a modified current source inverter. The control strategy consists in two PI controllers and dq transformation.
- The paper [57] presents a flyback dc-dc converter with line-frequency inverter. The control strategy consists in a inverse model with a single closed-loop PI controller.
- The paper [58] presents a boost-half-bridge dc-dc converter and full-bridge inverter. The control technique consists in a repetitive current controller based on fourth-order linear phase IIR filter. The repetitive current controller is used to reduce the total harmonic distortion and current regulation. There is a PI controller in the dc-dc stage.
- The paper [59] presents a flyback-based partial power dc-dc converter with a H-bridge inverter. The control strategy consists in a cascaded control loop (PI controllers)

for dc-dc stage and a classical single-phase voltage oriented control algorithm for dc-ac stage.

- The paper [60] presents a coupled inductor based cuk dc-dc converter connected to the line frequency current unfolding stage. The control strategy is comprised of different PI controllers.
- The paper [61] presents a LLC dc-dc converter connected to a full-bridge inverter. The control strategy of dc-ac stage consists in a dead-beat scheme. The control strategy of dc-dc stage consists in a simple closed-loop PI control.

3.2. Island Mode

In [62] a microinverter is presented and it consists of a high frequency dc-ac converter based on a dual active bridge (DAB) operating with zero-voltage-switching (ZVS) (Figure 22). The control strategy is presented in Figure 23 and it consists of three objectives: dc-link voltage v_{dc} regulation, power decoupling, and ac output voltage v_o regulation. First, the dc voltage is regulated by a PI controller that generates the average phase shift signal δ_{av} . The result is added to the ac offset signal δ_{ac} to generate the offset signal δ . Second, a power decoupling controller generates the ac phase shift δ_{ac} . It consists of a resonant controller to eliminate oscillations. Finally, two resonant drivers regulate the output ac voltage v_o and are adjusted to reject third order harmonics and to compensate for the effects of second order.

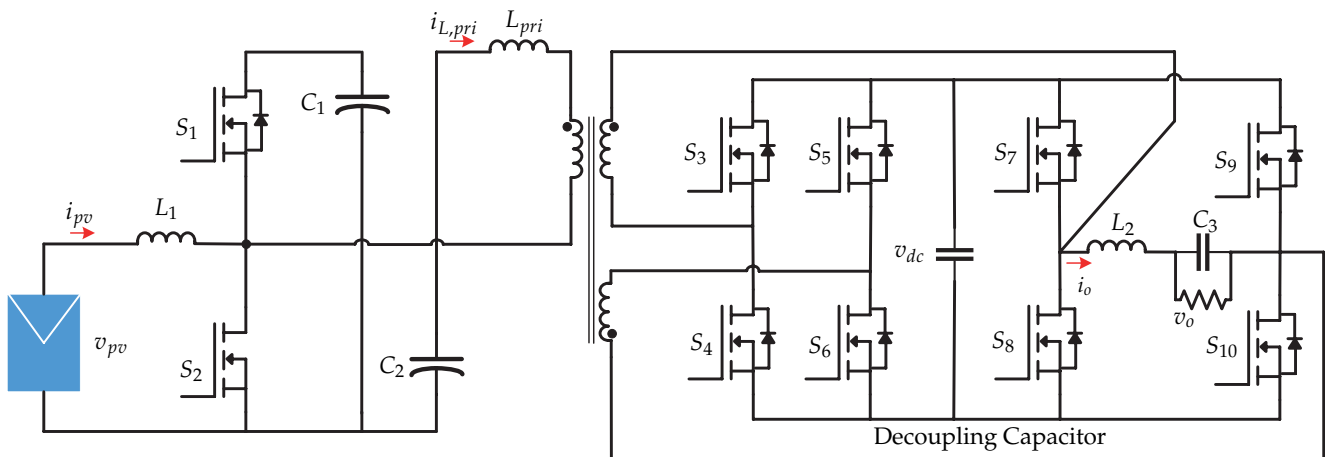


Figure 22. Microinverter's topology proposed in [62].

In [63], a microinverter comprises a dc-dc flyback converter coupled to an active decoupling circuit and a full-bridge inverter (Figure 24). This can operate in island mode and it is modulated by the pulse density (PDM). Its advantages are: use of electrolytic capacitors of low magnitude and it can operate in soft switching frequency. The proposed control strategy is presented in Figure 25 and is implemented in a Field Programmable Gate Array. The strategy consists of two control loops that control the dc-dc converter and control the full-bridge inverter. The control of the dc-dc stage consists of a voltage controller of the decoupling circuit that generates an input current reference i_{pv}^* which is compared with the current of the photovoltaic panel i_{pv} . The current controller generates the modulator for the switching sequence. Both controllers mentioned above are PI. On the other hand, the control of the dc-ac stage consists of a voltage controller whose input signal is the comparison of the load voltage v_o with the reference voltage v_o^* . The controller output is processed by the pulse density modulation generator and generates the pulse sequence for the decoupling circuit and for the single-phase voltage source inverter.

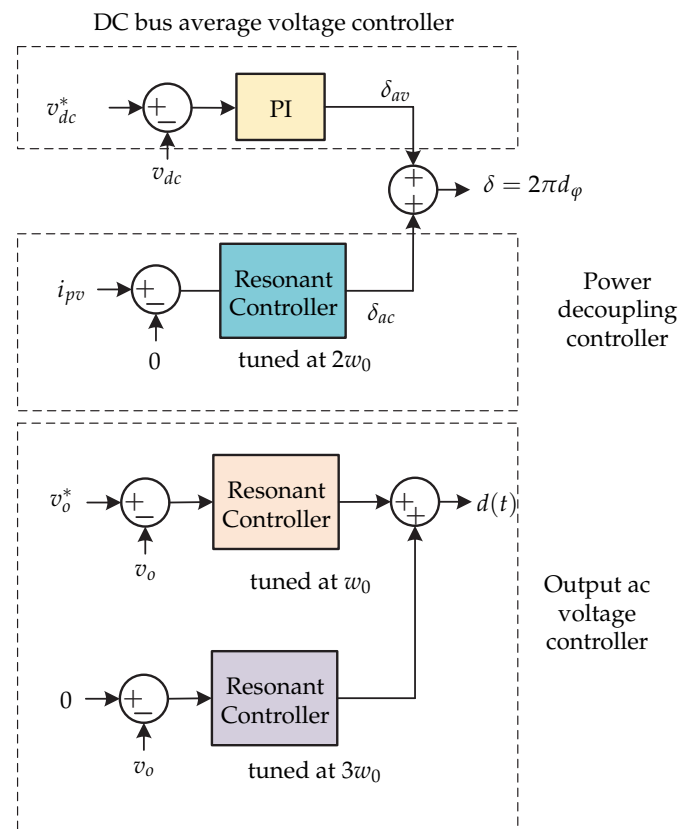


Figure 23. Control strategy proposed in [62].

3.3. Reactive Power Compensation

In [64], a microinverter is introduced and provides Volt/VAR support to the power grid. The microinverter consists of a first stage with a partial power LLC resonant converter followed by an interleaved full-bridge inverter (Figure 26). The control strategy is presented in Figure 27. First, there is an MPPT algorithm to extract the maximum power from the photovoltaic panel and generate the reference voltage v_{pv}^* , which is compared to the voltage of the photovoltaic panel v_{pv} . The error is processed by a PI controller and generates the phase-shift angle φ . In addition, to minimize the phase-shift angle, a switching frequency feedforward loop is implemented, which is generated by the voltage of the dc link v_{dc} , by the output power of the photovoltaic panel P_{pv}^* and by the reference voltage of the photovoltaic panel. This allows the dc-dc converter to change its switching frequency to maintain soft switching f_{sw_LLC} as well as to obtain an appropriate gain. In the dc-ac stage there is a double loop control. The outer voltage loop consists of the dc-link voltage regulation and is compared with a dc reference voltage v_{dc}^* obtained from a generator as a function of the output power of the photovoltaic panel and the voltage v_{pk} . The error is minimized by a PI controller that generates the reference current in the d -frame i_d^* . Then, a feedforward loop in terms of the output power of the photovoltaic panel and the voltage v_{pk} is added to the reference current. Both currents are added in d and q frame to generate the reference current i_g^* . Then the reference current is compared with the grid current and the error is minimized by a PI and resonant control (RC) to generate the duty cycle of the inverter.

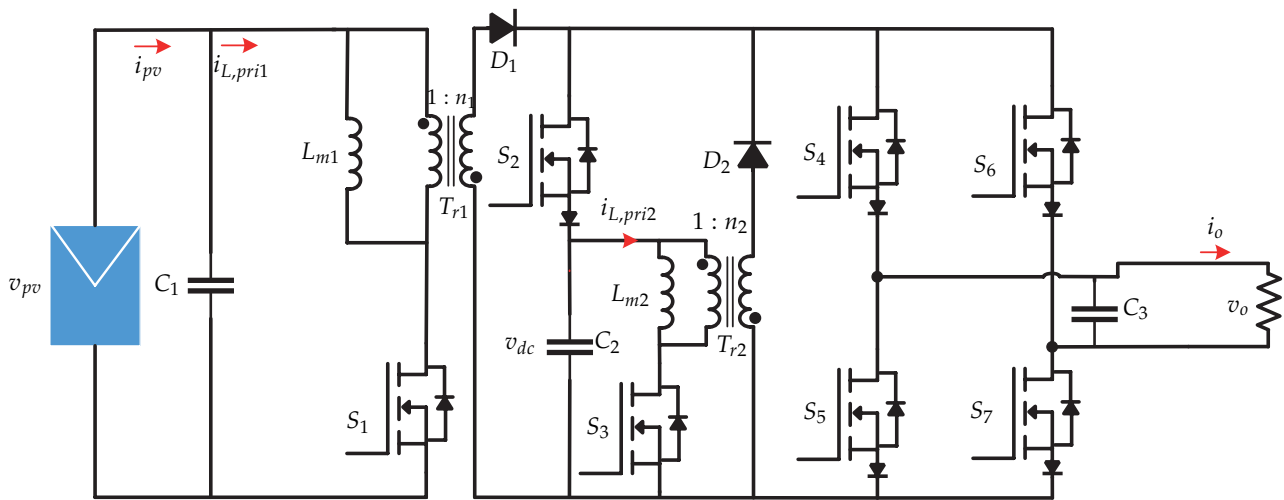


Figure 24. Microinverter's topology proposed in [63].

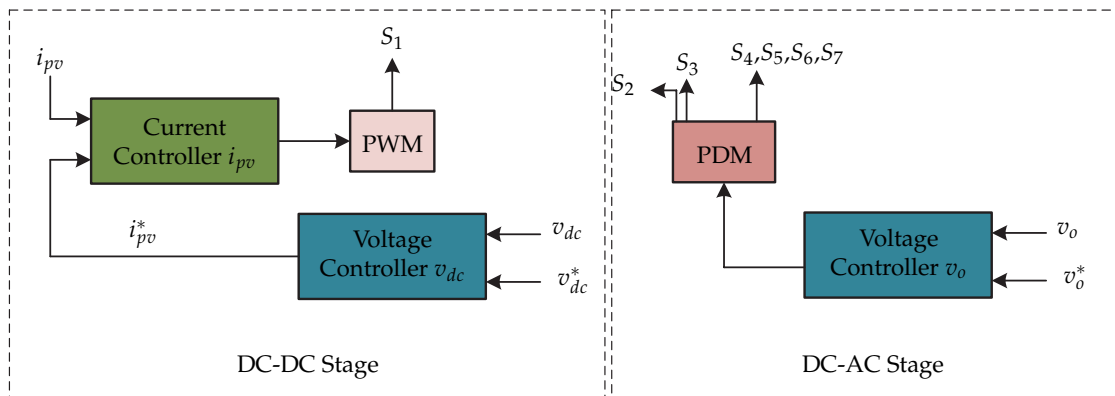


Figure 25. Control strategy proposed in [63].

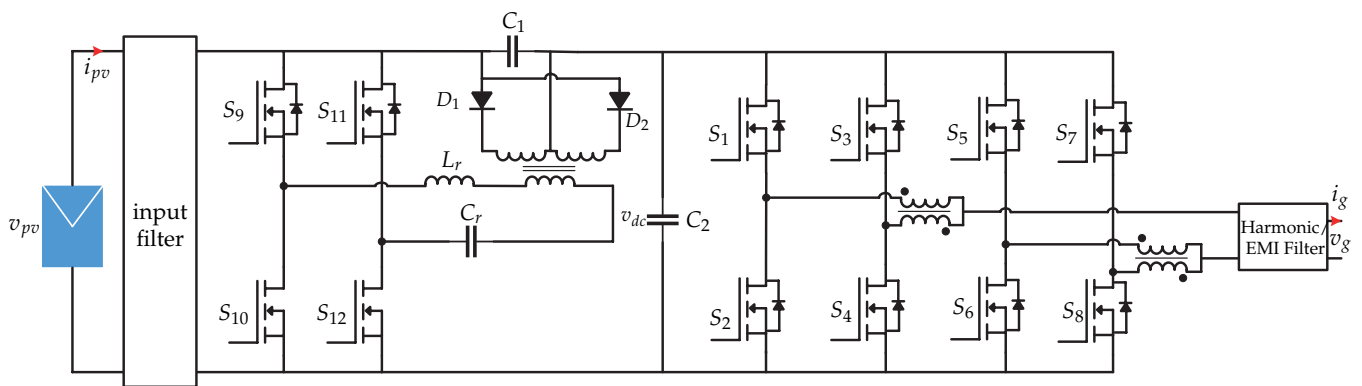


Figure 26. Microinverter's topology proposed in [64].

flyback converter and is subtracted from the duty cycle of the second flyback converter. The photovoltaic panel current is equal to the sum of the currents of the primary flyback converter and secondary flyback converter. Figure 32 shows the control strategy of the current injection circuit and it consists of a PI current controller that compares the inductor current of the third harmonic (i_y) with a reference current i_y^* . The reference current is obtained by the angle of the grid voltage θ_m (generated by a PLL), plus the reference power P^* (obtained by the sum of all the electrical powers of the photovoltaic panels), plus the desired output angle φ . $G_p(s)$ is the transfer function of the current injection circuit of the third harmonic.

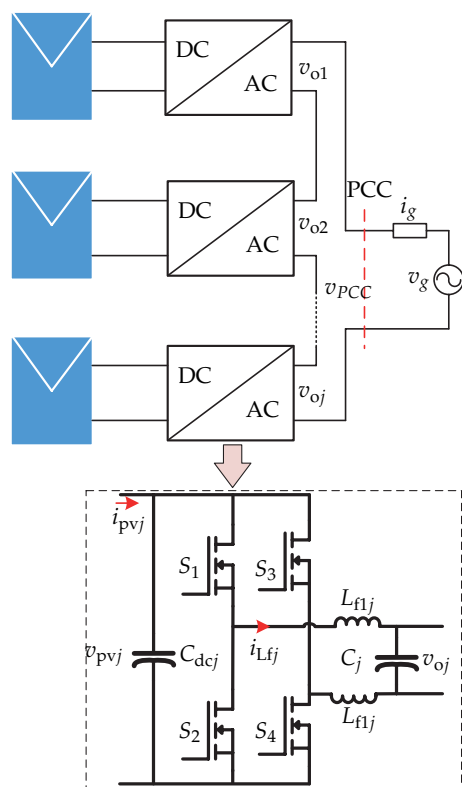


Figure 28. Microinverter's topology proposed in [65].

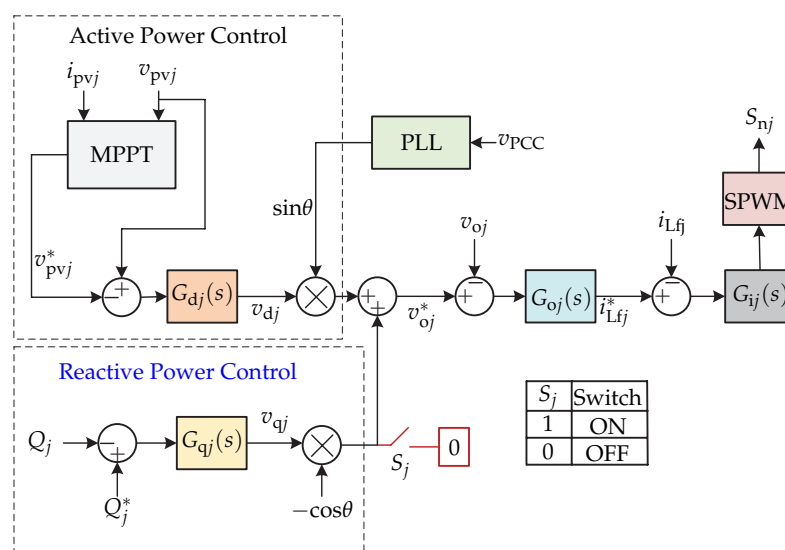


Figure 29. Control strategy proposed in [65].

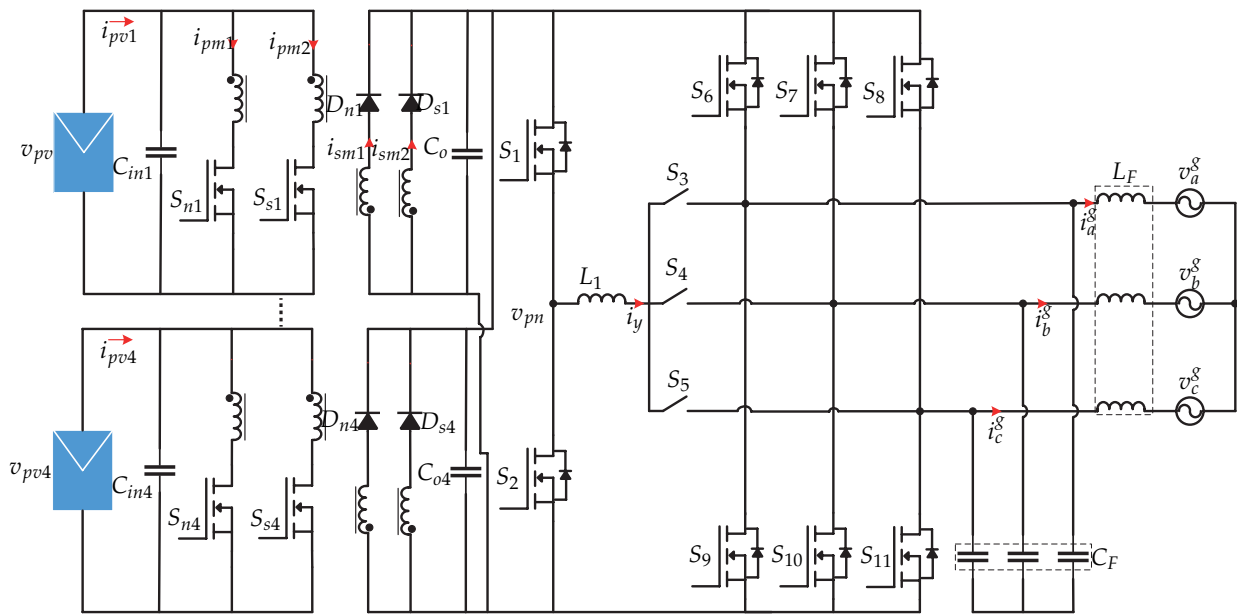


Figure 30. Microinverter’s topology proposed in [66].

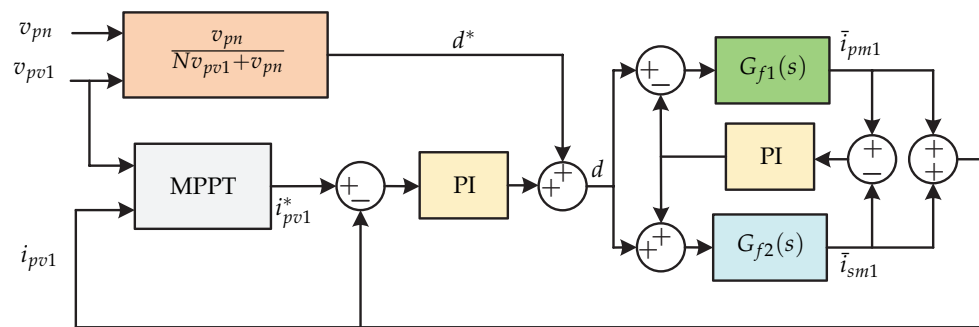


Figure 31. Control strategy of the MPPT proposed in [66].

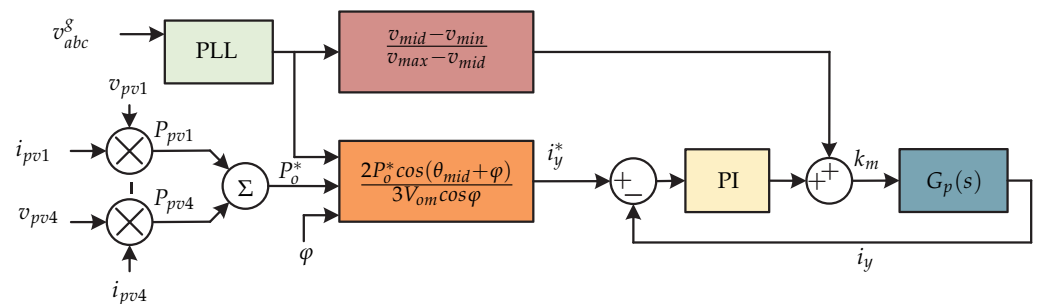


Figure 32. Control strategy proposed in [66].

In [25] a control strategy is presented to compensate the reactive power and is presented in Figure 33. This consists mainly of an MPPT algorithm that generates the reference current in d frame (i_d^*). Then, the currents i_d^* and i_q^* are multiplied by $\cos(\omega t)$ and $\sin(\omega t)$ respectively, whose angle is obtained by a PLL. Both reference currents are summed and compared with the grid current i_g that multiplied by a proportional gain k_{pg} generates the variation of the duty cycle ΔD . The duty cycle variation plus the nominal duty cycle generates the PWM signal.

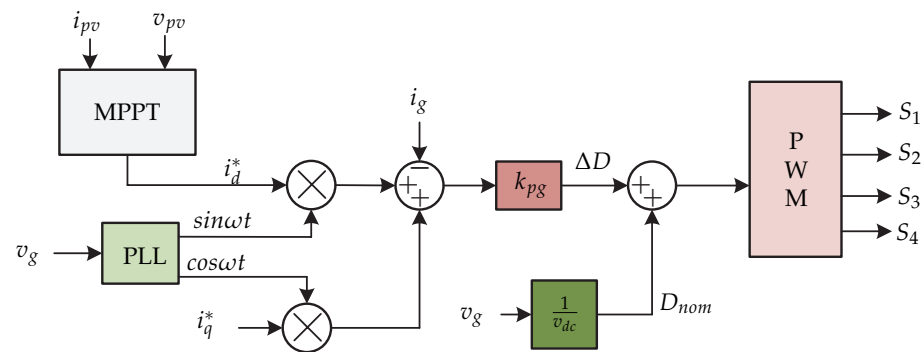


Figure 33. Control strategy proposed in [25].

Other control techniques are as follows:

- The paper [67] presents an active clamp flyback converter with a dual-buck inverter. The control consists of a current control (a 2-pole 2-zero compensator) for a dc-dc stage. The control technique in the dc-ac stage consists in a voltage-loop control (PI controller), a current-loop control (3-pole 3-zero compensator and feedback linearization), and a phase-locked loop. The power control is based a dq transformation.
- The paper [68] presents a two-stage microinverter and it consists of a bidirectional boost/buck dc-dc converter with coupled inductors and a full-bridge inverter. The control strategy consists of a conventional current control (PI controller) for reactive power compensation.
- The paper [69] presents a quasi Z-source (qZS) single-phase microinverter. The control strategy consists in a model predictive control with low-voltage ride-through capability.

3.4. Microinverter with Energy Storage

In [70] a microinverter with integrated storage is presented and it consists of a dual active H-bridge dc-dc converter (DAB); in addition, a dc-dc converter connected to a battery is coupled in parallel (Figure 34). This work only presents the connection stage of the photovoltaic panel and the battery with dc-link. The proposed dc-dc converter has two modes: on the first hand, it works as a dual-active H-bridge (DAB) converter, and on the second hand it works as a dual-transistor flyback converter. The proposed dual control strategy is presented in Figure 35. This consists of different conditions of the power flow P , which depending on the condition, the flyback mode or dual active H-bridge mode is selected. The article [70] does not present more details of the control strategy, it only mentions that the comparison between the power flow calculated with the reference is processed by a controller $G_{c2}(s)$ generating T_s , to then generate the switching sequence of the flyback mode. In the case of DAB mode, the controller $G_{c1}(s)$ generates an angle ϕ to regulate the power flow to/from the dc-ac stage. The multiplexer determines the sequence of commutation depending on the selected mode.

Other control techniques are as follows:

- The paper [71] presents a high-frequency push-pull topology with galvanic isolation with a voltage source inverter. The control technique consists of MPPT controller, a battery charge algorithm (constant current followed by constant voltage control), a dc-link voltage regulator (PI controller), and a current-loop control based a model predictive control.
- The paper [72] presents a dual-active bridge microinverter topology with integrated energy storage capability. The control strategy comprises a cascaded loop with two PI controllers and a two-loop approach with PI controller and PR controller.

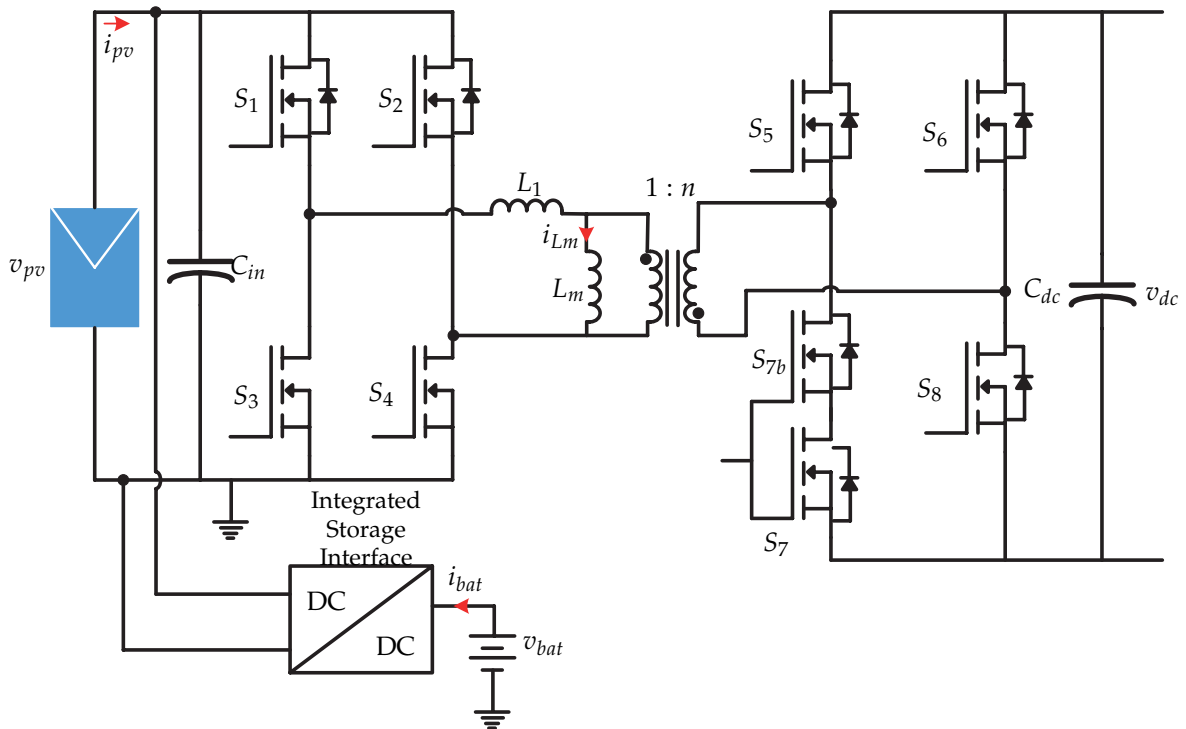


Figure 34. Microinverter’s topology proposed in [70].

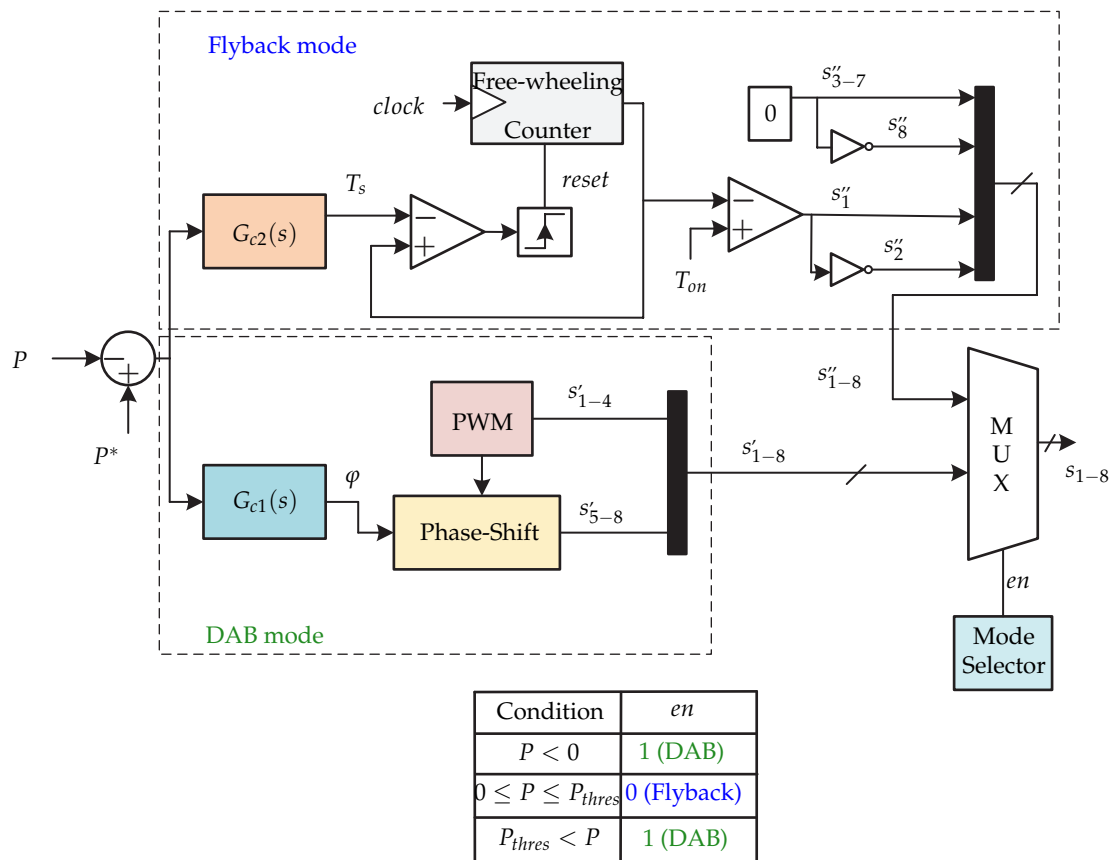


Figure 35. Control strategy proposed in [70].

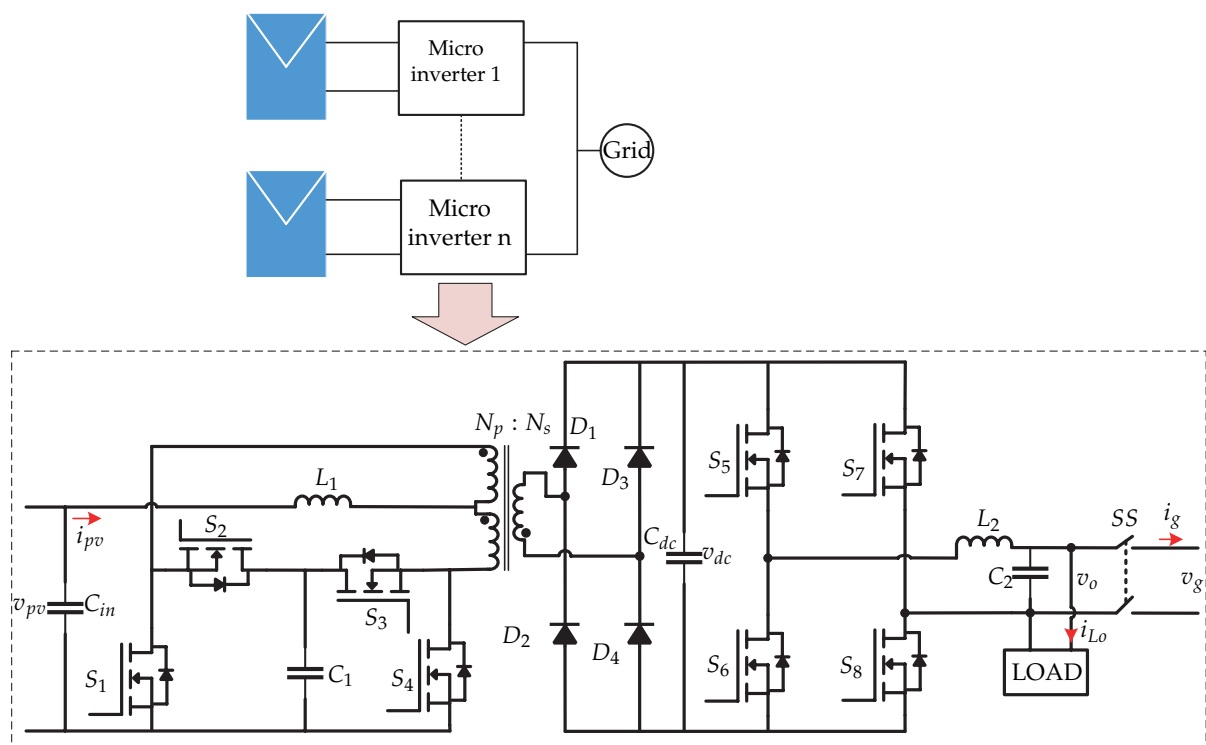


Figure 37. Microinverter's topology proposed in [73].

In [74–76] a dual-stage microinverter is presented and it consists of a push–pull dc–dc converter connected to a full-bridge inverter (Figure 38). The proposal of the article is a microinverter that can operate both in island mode and in mode connected to the electrical grid without the need to modify the control algorithm. In grid-connected mode, the microinverter must inject electrical power; on the other hand, in island mode, the microinverter must deliver an appropriate ac voltage to local loads. The control strategy of Figure 39 for the grid-connected mode consists of an internal loop that controls the injection of current i_{L_o} , while an external loop controls the voltage of the dc-link v_{dc} . In this case, the push–pull converter controls the MPPT algorithm, whose reference voltage v_{pv}^* is compared with the voltage of the photovoltaic panel v_{pv} that is processed by a voltage controller. In addition, the proposed control in the dc–dc stage limits the transformer current to avoid its saturation.

On the other hand, in Figure 40, the control strategy in island mode is presented. In island mode, the inner current loop does not change with respect to the aforementioned, but the outer voltage loop regulates the output voltage v_o (voltage source control algorithm). This is compared to a reference voltage v_o^* , generated by a droop control as a function of active and reactive power. The control of the dc–dc stage controls the voltage in the dc link by means of a voltage controller generating the limit of the reference voltage and is added to the reference voltage of the photovoltaic panel. All voltage controllers are PI, while current controllers are PR. The characteristic of the proposed reconfigurable control is that there are no transients between the microinverter and the load when switching from one mode to another.

Other control techniques are as follows:

- The paper [77] presents a two-stage microinverter and it consists of dc–dc triple active bridge (TAB) converter that integrates back-up battery; and the second stage is a voltage source inverter (VSI) that operates in both grid-connected mode (GCM) and stand-alone mode (SAM). The control algorithm consists in a central control based in a mode transition scheme. Each mode has PI controllers to regulate the current grid, current load, and dc-link voltage; it has a PR controller to regulate the load voltage.

- The paper [78] presents a buck-boost dc-dc converter cascaded interleaved flyback dc-dc converter with a unfolding bridge inverter. The control technique consists in a droop control and a peak current control.
- The paper [79] presents a current-fed push-pull, full-wave rectifier with full-bridge. The microinverter can operate in island mode and grid mode. The control technique comprises of different PI controllers for both modes.

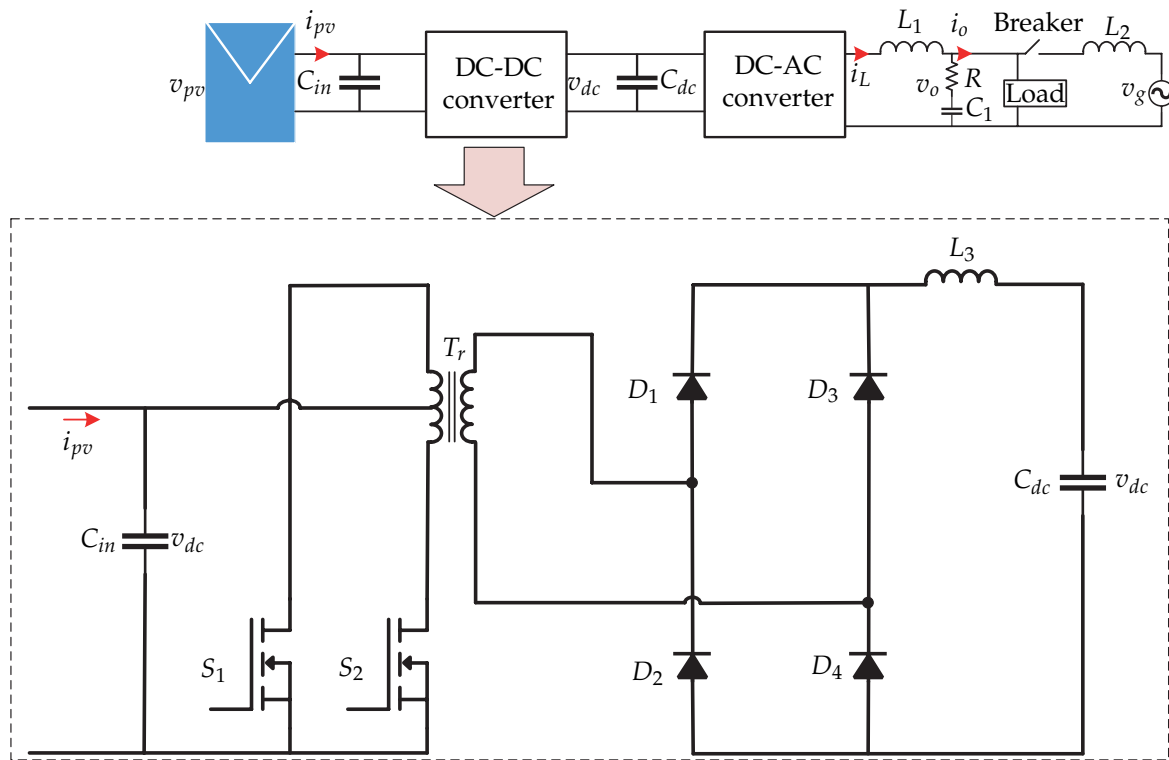


Figure 38. Microinverter's topology proposed in [74–76].

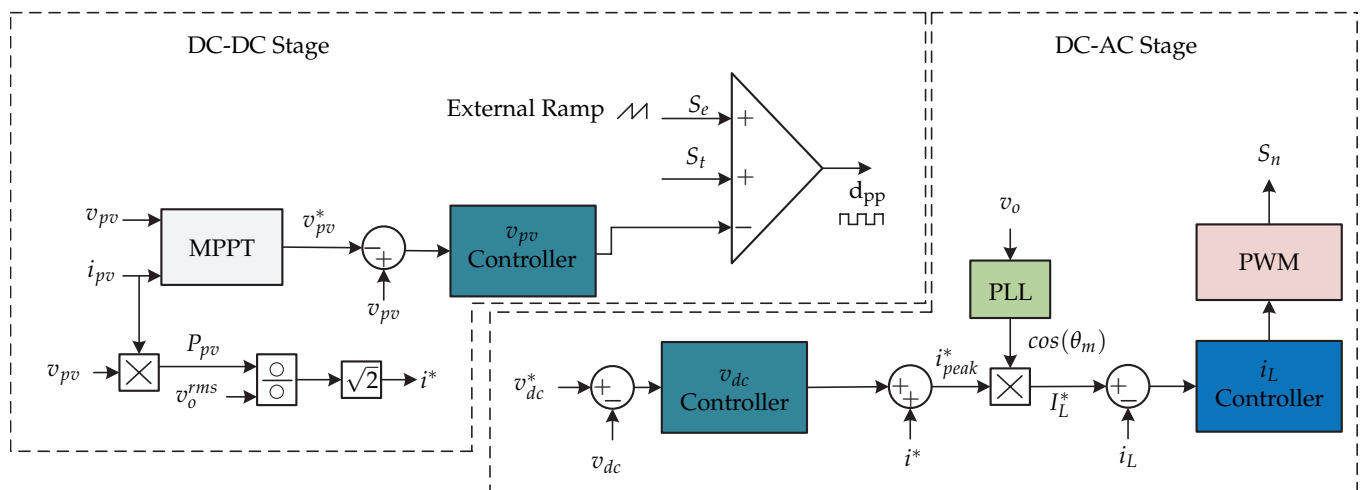


Figure 39. Control strategy proposed in [74–76].

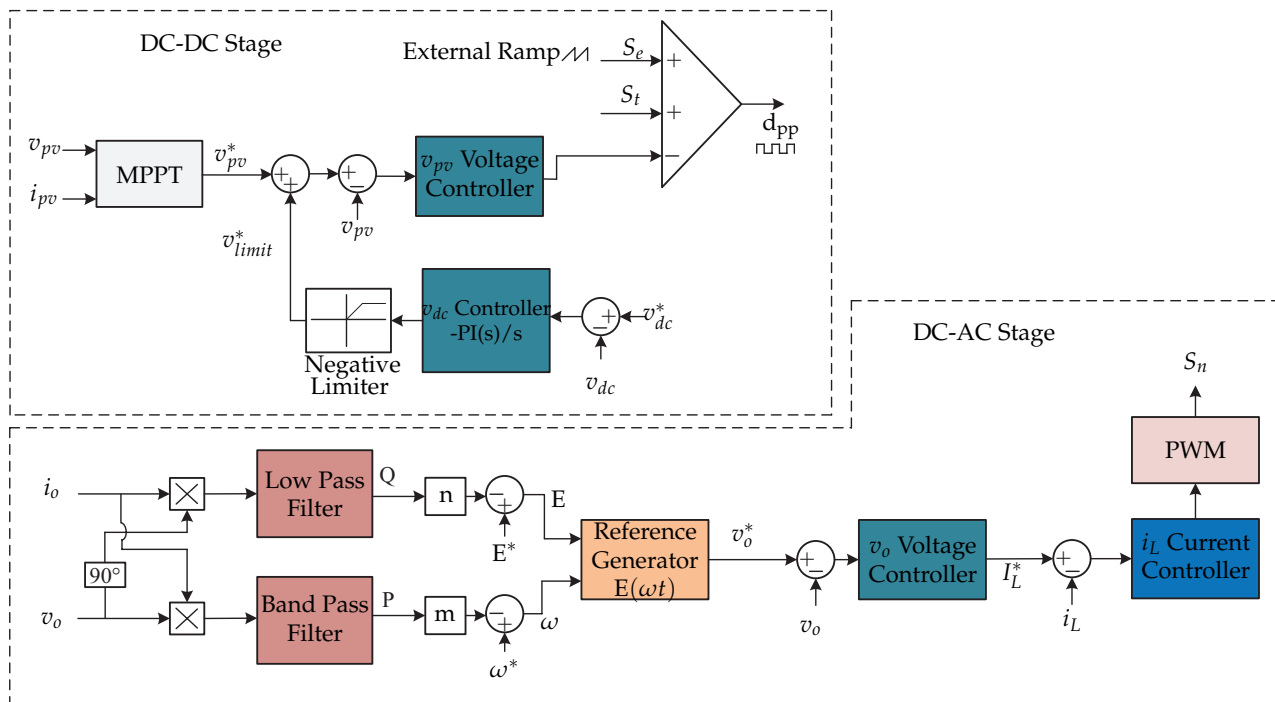


Figure 40. Control strategy proposed in [74,75].

4. Discussion

Table 1 presents the characteristics of the revised control strategies, in order to make a comparison between them. Table 1 shows the stability results as a function of the gain margin (GM) and phase margin (PM). In addition, the quality of the signals is presented as a function of the total harmonic distortion (THD) and the dynamic responses are also presented as a function of the settling time (t_s) in millisecond and the overshoot (M_p). In addition, the efficiency of the maximum power point tracking algorithm (MPPT) is presented.

Most of the authors use a PI controllers because they are simple and easy to design. As the microinverters are non-linear systems, the PI control is capable of working properly only in a reduced operating region, this being a disadvantage of the controller. In addition, it is necessary to determine the gain values of the controller, which is sensitive to variations and uncertainty of the microinverter parameters [80]. In addition, the revised articles tend to use the PR control that has better performance in the regulation of alternating current as compared to the PI control [81]; however, it also has the problem of sensitivity to variations and uncertainties. From this point of view, a feasible solution is to implement other control techniques, such as model-based predictive control [82], feedback linearization control [83], and fuzzy logic control [84].

In addition, as can be seen in Table 1, the different characteristics depend on both the topology (design) and the control strategy. The design determines the values of the various components contained in the microinverter to meet voltage and current requirements and also determines the size of the microinverter. In addition, this determines the voltage and current ratings of the power semiconductors. The selection of electronic components will mainly influence the efficiency of the microinverter. Finally, once the topology is designed and the components are selected, it is necessary to regulate the voltage and current levels despite the presence of disturbances. Therefore, it is necessary to implement control techniques that ensure a correct operation of the microinverter to meet the different voltage and current requirements and thereby increase the reliability and robustness of the microinverter.

Table 1. Characteristics of the revised control strategies.

Cite	GM(dB)	PM	THD(%)	t_s (ms)	M_p	MPPT(%)	Advantage	Topology	Controller
[12]	-	-	$4.37(i_g)$	-	-	-	Low frequency Harmonic mitigation. Switching losses reduction.	Full bridge inverter	Hysteresis + PR
[13]	-	-	$2.87(i_g)$ $3.09(v_g)$	$20(i_g)$	-	99.7	High reliability Wide operating range. Fast MPPT.	Boost-half-bridge converter + full-bridge inverter	PI controllers + Resonant control
[15]	$12(i_g)$ $\inf(v_{dc})$	$58^\circ(i_g)$ $74^\circ(v_{dc})$	$2.5(i_g)$	-	-	-	Fast dynamic response.	LLC resonant converter + 3-phase dc-ac converter	PI Controllers
[18]	$\inf(i_{L2})$	$85.9^\circ(i_{L2})$	$3.18(i_g)$	-	-	96	High reliability. Reactive power support. LVRT Capacity.	Non-inverted Cuk connected to an inverter Cuk converter	PI and PR controllers
[19]	-	-	-	-	-	98.5	Ability to estimate current for different inductance values. Elimination of measurement noise.	Flyback converter + VSI	PI control + PCM + State Observer
[21]	-	-	Off-grid $0.5(v_g)$ On-grid $2.4(i_g)$	-	-	-	LVRT and anti-island capability.	Flyback converter + VSI	PI controllers + DQ power estimation
[25]	-	-	$3.8(i_g)$	-	-	-	High conversion efficiency High reliability	Flyback converter + series resonant voltage doubler	P controller + feedback linearization + Voltage controller
[26]	-	-	$3(i_g)$	-	-	-	Simple. Elimination of distortion caused by zero crossing.	Coupled-inductor double-boost inverter	PI controllers

Table 1. Cont.

Cite	GM(dB)	PM	THD(%)	t_s (ms)	M_p	MPPT(%)	Advantage	Topology	Controller
[27]	-	-	-	$10(v_o)$	$5V(v_o)$	-	Switching losses reduction.	DMR based series resonant dc-dc converter	PI controllers
[62]	-	-	0	$70(v_{dc})$	-	-	ZVS capacity. Switching losses reduction. Decoupling capacitance reduction.	Flyback converter + VSI	PR control + HC
[29]	$\inf(i_o)$	$45^\circ(i_o)$	$2.4(i_o)$	-	-	-	Fast dynamic response Harmonic frequencies elimination. Low computational burden. Elimination of disturbances. Hybrid operation(DCM-CCM).	DAB inverter	PI + RC controllers
[63]	-	$60^\circ(i_{pv})$ $60^\circ(v_{dc})$ $60^\circ(v_o)$	$3.73(i_o)$	$1000(v_{dc})$	-	-	ZCS switching capacity. Wide range of input voltages.	Flyback + active decoupling circuit + full-bridge inverter	PI controllers
[64]	-	-	-	-	-	-	Reactive power support. High Efficiency	LLC resonant converter + interleaved full-bridge inverter	PI controllers + RC + feedforward loop
[65]	-	-	-	-	-	-	Distributed control. Active and reactive power control capacity.	Cascaded full-bridge inverter	Distributed control: P + PI + PR controllers
[66]	-	-	Full load $4.29(i_o)$ Partial load $6.82(i_o)$	-	-	-	Controllable power factor. High efficiency. Independent MPPT control.	Interleaved flyback converter + 3-phase Current Source Inverter	PI controllers
[70]	-	-	-	$0.04(i_{pv})$	$0.2 A(i_{pv})$	-	Two modes of operation Flyback and DAB. Reduction of switching losses. High stability.	DAB + dc-dc converter for the batteries	Dual-mode control
[73]	-	-	-	-	-	-	Multifunctionality. Parallel multi-mode operation.	Push-pull converter + full-bridge inverter	PI controllers

Table 1. Cont.

Cite	GM(dB)	PM	THD(%)	t_s (ms)	M_p	MPPT(%)	Advantage	Topology	Controller
[74,75]	-	On-grid 89.6°(v_{pv}) 58.6°(i_g) 87°(v_{dc}) Off-grid 90.2°(v_{pv}) 65.2°(v_o) 76.2°(v_{dc}) 81.2°(i_o)	0.05 s(v_g)	-	-	-	Ability to operate off-grid and on-grid. Reconfigurable Control.	Push-pull converter + full-bridge inverter	PI + PR controllers

5. Conclusions

This article presented an overview of microinverters and a review of control strategies for applications such as grid-connected, island mode, reactive power compensation, incorporation of energy storage, and multi-modes. Microinverters are a promising solution to mitigate the problems of using photovoltaic panels, such as partial shading. Within the reviews it can be inferred that there is an increase of studies on microinverters, due to the advancement of semiconductor technology as well as cost reduction. From the point of view of the control strategy, research tends to use PI controllers and PR.

The control strategies were studied for the different applications in microinverters. The proposed control strategy was described as well as the associated power converters. It can be mentioned that due to the advancement of microprocessors, it is tending to the incorporation of multiple controls and multiple modes in the microinverters, increasing reliability and functionality of the photovoltaic system.

Finally, it can be mentioned that although the design and selection of the electronic components in a power converter topology is important and essential in the conversion efficiency, the design of the control strategy is a third important factor in increasing the reliability and functionality of microinverters.

Funding: This work was supported by the Chilean Government under Project CONICYT/FONDECYT 1191028, ANID Becas/Doctorado Nacional 21201878, and Universidad of Talca.

Institutional Review Board Statement: Not applicable.

Informed Consent Statement: Not applicable.

Data Availability Statement: Not applicable.

Conflicts of Interest: The authors declare no conflict of interest.

Abbreviations

The main abbreviations and nomenclatures that are used in this manuscript are listed below:

ACC	Phase Accumulator
DAB	Dual active bridge
DMR	Dual Mode Rectifier
CVT	Constant Voltage Method
EMI	Electromagnetic Interference
GCM	Grid Connected Mode
GM	Gain Margin
HC	Harmonic Compensator
LIM	Line-interactive Mode
PCM	Peak Current Control
PDM	Pulse Density Modulator
PM	Phase Margin
SAM	Standalone Mode
RC	Repetitive Controller
THD	Total Harmonic Distortion
ZVS	Zero Voltage Switching
A_m	Voltage amplitude reference
C_{dc}	DC-link capacitor
C_F	Filter capacitor
C_{in}	Input capacitor
C_x	Capacitor $x = 1, 2, \dots$
C_o	Output capacitor
C_r	Resonant capacitor
d	Duty cycle
D_{CCM}	Duty cycle in continuous conduction mode

D_{DCM}	Duty cycle in discontinuous conduction mode
D_n	Diode n , where $n = 1, 2, \dots$
D_{nj}	Diode n of the microinverter $j = 1, 2, \dots$
D_{nom}	Rated duty cycle
D_p	Hybrid nominal duty ratio
d_{pp}	Switching signal pattern
E	Amplitude of the inverter voltage
en	Enable the mode selector
f^*	Reference of switching frequency
f_o	Sampling frequency
f_s	Switching frequency
$G(s)$	Transfer function
i_{bat}	Battery current
i_{Cn}	Current of capacitor $n = 1, 2, 3, \dots$
i_d	d Frame current
$i_g(t)$	Grid current
I_g^*	Amplitude of the grid current reference
i_L	Inductor current
i_{l_o}	Load current
$i_{L,pri}$	Current of the primary side transformer
$i_{L,sec}$	Current of the secondary side transformer
i_{lim}	Current amplitude limit reference
i_{pv}	Photovoltaic panel current
\hat{I}_{pv}	Estimated photovoltaic panel current
i_o	Output current
i_q	q Frame current
k	Sensor gain
K_d	Derivative gain
k_m	Duty ratio
k_{pg}	Proportional gain
L_F	Filter inductor
L_{in}	Input inductor
L_m	Magnetizing inductor
L_n	Inductor n , where $n = 1, 2, 3, \dots$
L_{on}	Output inductor n , where $n = 1, 2, \dots$
L_s	Inductor of transformer
L_r	Resonant inductor
m	Amplitude droop coefficient
m_x	Modulator signal $x = a, b, c$
M_p	Overshoot
n	Frequency droop coefficient
p_o	Output power of the inverter
P^*	Power reference
P	Active power
P_{pv}	Photovoltaic panel power
Q	Reactive power
R	Resistor
s_{1-8}	Gating voltages for switches S_{1-8}
S_n	Switch n , where $n = 1, 2, 3, \dots$
T_{on}	Fixed on-time
t_s	Settling time
T_s	Switching period
v_{ab}	Inverter voltage
v_{bat}	Battery voltage
v_{cd}	Voltage between the terminals cd
v_d	Voltage in the d frame
v_{dc}	DC-link voltage
v_{Cn}	Voltage of capacitor $n = 1, 2, 3, \dots$

v_g	Grid voltage
v_{mpp}	Voltage in the maximum power point
v_{max}	Maximum value of the dc-link voltage
v_{mid}	Medium value of the dc-link voltage
v_{min}	Minimum value of the dc-link voltage
v_{limit}^*	Limit voltage reference
v_o	Output voltage
V_{om}	Magnitude of the output phase voltage.
v_{PCC}	Voltage in the point common coupling
v_{pv}	Photovoltaic panel voltage
v_q	Voltage in the q frame
Δ	Disturbance or variation
φ	Output angle
δ	Offset signal
θ_m	Angle of the grid voltage
ω	Frequency of the inverter voltage

References

- Kouro, S.; Leon, J.I.; Vinnikov, D.; Franquelo, L.G. Grid-Connected Photovoltaic Systems: An Overview of Recent Research and Emerging PV Converter Technology. *IEEE Ind. Electron. Mag.* **2015**, *9*, 47–61. [\[CrossRef\]](#)
- Masson, G.; Kaizuka, I. Trends in Photovoltaic Applications 2020. International Energy Agency Photovoltaic Power System Report. 2020; ISBN 978-3-907281-01-7. Available online: https://iea-pvps.org/wp-content/uploads/2020/11/IEA_PVPS_Trends_Report_2020-1.pdf (accessed on 25 August 2021).
- Yan, Y.; Xiang, L.; Dianfeng, W. Integrated Solutions for Photovoltaic Grid Connection: Increasing the Reliability of Solar Power. *IEEE Power Energy Mag.* **2014**, *12*, 84–91. [\[CrossRef\]](#)
- Anzalchi, A.; Sundararajan, A.; Moghadasi, A.; Sarwat, A. High-Penetration Grid-Tied Photovoltaics: Analysis of Power Quality and Feeder Voltage Profile. *IEEE Ind. Appl. Mag.* **2019**, *25*, 83–94. [\[CrossRef\]](#)
- Freddy, T.K.S.; Rahim, N.A. *Photovoltaic Inverter Topologies for Grid Integration Applications*; Springer: Berlin/Heidelberg, Germany, 2016; pp. 13–42.
- Yang, Y.; Kim, K.; Blaabjerg, F.; Sangwongwanich, A. *Advances in Grid-Connected Photovoltaic Power Conversion Systems*; Woodhead Publishing: Shaxton, UK, 2018.
- Ikkurti, H.P.; Saha, S. A comprehensive techno-economic review of microinverters for Building Integrated Photovoltaics (BIPV). *Renew. Sustain. Energy Rev.* **2015**, *47*, 997–1006. [\[CrossRef\]](#)
- Alluhaybi, K.; Batarseh, I.; Hu, H. Comprehensive Review and Comparison of Single-Phase Grid-Tied Photovoltaic Microinverters. *IEEE J. Emerg. Sel. Top. Power Electron.* **2020**, *8*, 1310–1329. [\[CrossRef\]](#)
- Xiao, W.; Moursi, M.; Khan, O.; Infield, D. A Review of Grid-Tied Converter Topologies Used in Photovoltaic Systems. *Renew. Power Gener. IET* **2016**, *10*, 1543–1551.
- Sher, H.A.; Addoweesh, K.E. Micro-inverters—Promising solutions in solar photovoltaics. *Energy Sustain. Dev.* **2012**, *16*, 389–400. [\[CrossRef\]](#)
- Garcia-Rodriguez, L.; Jones, V.; Balda, J.; Lindstrom, E.; Oliva, A.; Gonzalez-Llorente, J. Design of a GaN-based microinverter for photovoltaic systems. In Proceedings of the 2014 IEEE 5th International Symposium on Power Electronics for Distributed Generation Systems (PEDG), Galway, Ireland, 24–27 June 2014; pp. 1–6. [\[CrossRef\]](#)
- Zhang, H.; Li, X.; Xiao, S.; Balog, R.S. Hybrid hysteresis current control and low-frequency current harmonics mitigation based on proportional resonant in dc/ac inverter. *IET Power Electron.* **2018**, *11*, 2093–2101. [\[CrossRef\]](#)
- Jiang, S.; Cao, D.; Li, Y.; Peng, F.Z. Grid-Connected Boost-Half-Bridge Photovoltaic Microinverter System Using Repetitive Current Control and Maximum Power Point Tracking. *IEEE Trans. Power Electron.* **2012**, *27*, 4711–4722. [\[CrossRef\]](#)
- Jiang, S.; Cao, D.; Peng, F.Z.; Li, Y. Grid-connected boost-half-bridge photovoltaic micro inverter system using repetitive current control and maximum power point tracking. In Proceedings of the 2012 Twenty-Seventh Annual IEEE Applied Power Electronics Conference and Exposition (APEC), Orlando, FL, USA, 5–9 February 2012; pp. 590–597. [\[CrossRef\]](#)
- Chen, L.; Hu, C.; Zhang, Q.; Zhang, K.; Batarseh, I. Modeling and Triple-Loop Control of ZVS Grid-Connected DC/AC Converters for Three-Phase Balanced Microinverter Application. *IEEE Trans. Power Electron.* **2015**, *30*, 2010–2023. [\[CrossRef\]](#)
- Chen, L.; Amirahmadi, A.; Zhang, Q.; Kutkut, N.; Batarseh, I. Design and Implementation of Three-Phase Two-Stage Grid-Connected Module Integrated Converter. *IEEE Trans. Power Electron.* **2014**, *29*, 3881–3892. [\[CrossRef\]](#)
- Chen, F.; Zhang, Q.; Amirahmadi, A.; Batarseh, I. Modeling and analysis of DC-link voltage for three-phase four-wire two-stage micro-inverter. In Proceedings of the 2014 IEEE Applied Power Electronics Conference and Exposition-APEC 2014, Fort Worth, TX, USA, 16–20 March 2014; pp. 3000–3005. [\[CrossRef\]](#)
- Rajeev, M.; Agarwal, V. Analysis and Control of a Novel Transformer-Less Microinverter for PV-Grid Interface. *IEEE J. Photovoltaics* **2018**, *8*, 1110–1118. [\[CrossRef\]](#)

19. Falconar, N.; Beyragh, D.S.; Pahlevani, M. An Adaptive Sensorless Control Technique for a Flyback-Type Solar Tile Microinverter. *IEEE Trans. Power Electron.* **2020**, *35*, 13554–13562. [\[CrossRef\]](#)
20. Falconar, N.; Beyragh, D.S.; Pahlevani, M. A novel control system for solar tile micro-inverters. In Proceedings of the 2018 IEEE Applied Power Electronics Conference and Exposition (APEC), San Antonio, TX, USA, 4–8 March 2018; pp. 375–380. [\[CrossRef\]](#)
21. Öztürk, S.; Çadircı, I. A Generalized and Flexible Control Scheme for Photovoltaic Grid-Tie Microinverters. *IEEE Trans. Ind. Appl.* **2018**, *54*, 505–516. [\[CrossRef\]](#)
22. Öztürk, S.; Çaditoi, I. A generalized and flexible control scheme for photovoltaic grid-tie microinverters. In Proceedings of the 2015 International Conference on Renewable Energy Research and Applications (ICRERA), Palermo, Italy, 22–25 November 2015; pp. 699–703. [\[CrossRef\]](#)
23. Öztürk, S.; Çadircı, I. A generalized control approach for photovoltaic grid-tie microinverters. In Proceedings of the 2015 Intl Aegean Conference on Electrical Machines Power Electronics (ACEMP), 2015 Intl Conference on Optimization of Electrical Electronic Equipment (OPTIM) 2015 Intl Symposium on Advanced Electromechanical Motion Systems (ELECTROMOTION), Side, Turkey, 2–4 September 2015; pp. 800–806. [\[CrossRef\]](#)
24. Öztürk, S.; Çadircı, I. DSPIC microcontroller based implementation of a flyback PV microinverter using Direct Digital Synthesis. In Proceedings of the 2013 IEEE Energy Conversion Congress and Exposition, Denver, CO, USA, 15–19 September 2013; pp. 3426–3433. [\[CrossRef\]](#)
25. Cha, W.; Cho, Y.; Kwon, J.; Kwon, B. Highly Efficient Microinverter With Soft-Switching Step-Up Converter and Single-Switch-Modulation Inverter. *IEEE Trans. Ind. Electron.* **2015**, *62*, 3516–3523. [\[CrossRef\]](#)
26. Fang, Y.; Ma, X. A Novel PV Microinverter With Coupled Inductors and Double-Boost Topology. *IEEE Trans. Power Electron.* **2010**, *25*, 3139–3147. [\[CrossRef\]](#)
27. Shen, Y.; Wang, H.; Shen, Z.; Yang, Y.; Blaabjerg, F. A 1-MHz Series Resonant DC–DC Converter With a Dual-Mode Rectifier for PV Microinverters. *IEEE Trans. Power Electron.* **2019**, *34*, 6544–6564. [\[CrossRef\]](#)
28. Shen, Y.; Wang, H.; Shen, Z.; Yang, Y.; Blaabjerg, F. Series Resonant DC-DC Converter With Dual-Mode Rectifier for PV Microinverters. In Proceedings of the 2018 International Power Electronics Conference (IPEC-Niigata 2018-ECCE Asia), Niigata, Japan, 20–24 May 2018; pp. 1788–1792. [\[CrossRef\]](#)
29. Lee, S.; Cha, W.; Kwon, J.; Kwon, B. Control Strategy of Flyback Microinverter With Hybrid Mode for PV AC Modules. *IEEE Trans. Ind. Electron.* **2016**, *63*, 995–1002. [\[CrossRef\]](#)
30. Yaqoob, S.J.; Obed, A.; Zubo, R.; Al-Yasir, Y.I.A.; Fadhel, H.; Mokryani, G.; Abd-Alhameed, R.A. Flyback Photovoltaic Micro-Inverter with a Low Cost and Simple Digital-Analog Control Scheme. *Energies* **2021**, *14*, 4239.
31. El Aroudi, A.; Debbat, M.; Al-Numay, M.; Abouloiafa, A. Fast-Scale Instability and Stabilization by Adaptive Slope Compensation of a PV-Fed Differential Boost Inverter. *Appl. Sci.* **2021**, *11*, 2106. [\[CrossRef\]](#)
32. Abdel-Rahim, O.; Alamir, N.; Abdelrahman, M.; Orabi, M.; Kennel, R.; Ismeil, M.A. A Phase-Shift-Modulated LLC-Resonant Micro-Inverter Based on Fixed Frequency Predictive-MPPT. *Energies* **2020**, *13*, 1460. [\[CrossRef\]](#)
33. Valderrama-Blavi, H.; Rodríguez-Ramos, E.; Olalla, C.; Genaro-Muñoz, X. Sliding-Mode Approaches to Control a Microinverter Based on a Quadratic Boost Converter. *Energies* **2019**, *12*, 3697. [\[CrossRef\]](#)
34. Dong, M.; Tian, X.; Li, L.; Song, D.; Wang, L.; Zhao, M. Model-Based Current Sharing Approach for DCM Interleaved Flyback Micro-Inverter. *Energies* **2018**, *11*, 1685. [\[CrossRef\]](#)
35. Hsieh, H.I.; Hou, J. Realization of Interleaved PV Microinverter by Quadrature-Phase-Shift SPWM Control. *IEEJ J. Ind. Appl.* **2015**, *4*, 643–649. [\[CrossRef\]](#)
36. Hsieh, H.I.; Hsieh, G.C.; Hou, J. Realization study of interleaved PV microinverter by quadrature-phase-shift SPWM control. In Proceedings of the 2014 International Power Electronics Conference (IPEC-Hiroshima 2014-ECCE ASIA), Hiroshima, Japan, 18–21 May 2014; pp. 526–531. [\[CrossRef\]](#)
37. Kim, K.S.; Jeong, S.G.; Kwon, B.H. Single power-conversion DAB microinverter with safe commutation and high efficiency for PV power applications. *Sol. Energy* **2019**, *193*, 676–683. [\[CrossRef\]](#)
38. Gaafar, M.A.; Ibrahim, E.A.; Orabi, M. Multi-input transformer-less four-wire microinverter with distributed MPPT for PV systems. *Int. J. Circuit Theory Appl.* **2021**, *49*, 1704–1725. [\[CrossRef\]](#)
39. Evran, F. Design and control of an LCL-type single-phase grid-connected inverter with inverter current feedback using the phase-delay method. *Turk. J. Electr. Eng. Comput. Sci.* **2019**, *27*, 4702–4714. [\[CrossRef\]](#)
40. Yahya, A.; El Fadil, H.; Oulcaid, M.; Ammeh, L.; Giri, F.; Guerrero, J.M. Control of Grid Connected Photovoltaic Systems with Microinverters: New Theoretical Design and Numerical Evaluation. *Asian J. Control.* **2018**, *20*, 906–918. [\[CrossRef\]](#)
41. Renaudineau, H.; Lopez, D.; Flores-Bahamonde, F.; Kouro, S. Flatness-based control of a boost inverter for PV microinverter application. In Proceedings of the 2017 IEEE 8th International Symposium on Power Electronics for Distributed Generation Systems (PEDG), Florianopolis, Brazil, 17–20 April 2017; pp. 1–6. [\[CrossRef\]](#)
42. Lopez, D.; Flores-Bahamonde, F.; Renaudineau, H.; Kouro, S. Double voltage step-up photovoltaic microinverter. In Proceedings of the 2017 IEEE International Conference on Industrial Technology (ICIT), Toronto, ON, Canada, 22–25 March 2017; pp. 406–411. [\[CrossRef\]](#)
43. Caiza, D.L.; Kouro, S.; Flores-Bahamonde, F.; Hernandez, R. Unfolding PV Microinverter Current Control: Rectified Sinusoidal vs Sinusoidal Reference Waveform. In Proceedings of the 2018 IEEE Energy Conversion Congress and Exposition (ECCE), Portland, OR, USA, 23–27 September 2018; pp. 7094–7100. [\[CrossRef\]](#)

44. Lopez, D.; Renaudineau, H.; Flores-Bahamonde, F.; Kouro, S. Evaluation of photovoltaic microinverter configurations based on different converter stages and step-up voltage ratios. In Proceedings of the 2017 19th European Conference on Power Electronics and Applications (EPE'17 ECCE Europe), Warsaw, Poland, 11–14 September 2017; pp. P.1–P.8. [\[CrossRef\]](#)
45. Vongkoon, P.; Liutanakul, P.; Wiwatcharagoses, N. Analysis and Design of DC Bus Voltage Control Regarding Third Harmonic Reduction and Dynamic Improvement for Half-Bridge Microinverter. In Proceedings of the 2018 15th International Conference on Electrical Engineering/Electronics, Computer, Telecommunications and Information Technology (ECTI-CON), Chiang Rai, Thailand, 18–21 July 2018; pp. 17–20. [\[CrossRef\]](#)
46. Lopez-Santos, O.; Garcia, G.; Martinez-Salamero, L.; Cortes-Torres, L. Suppressing the effect of the DC-link voltage ripple on the current control of a sliding-mode controlled microinverter. In Proceedings of the 2015 CHILEAN Conference on Electrical, Electronics Engineering, Information and Communication Technologies (CHILECON), Santiago, Chile, 28–30 October 2015; pp. 447–452. [\[CrossRef\]](#)
47. Lopez-Santos, O.; García, G.; Martínez-Salamero, L. Derivation of a global model of a two-stage photovoltaic microinverter using sliding-mode control. In Proceedings of the 2015 IEEE 13th Brazilian Power Electronics Conference and 1st Southern Power Electronics Conference (COBEP/SPEC), Fortaleza, Brazil, 29 November–2 December 2015; pp. 1–6. [\[CrossRef\]](#)
48. Sahu, P.K.; Shaw, P.; Maity, S. Modeling and control of grid-connected DC/AC converters for single-phase micro-inverter application. In Proceedings of the 2015 Annual IEEE India Conference (INDICON), New Delhi, India, 17–20 December 2015; pp. 1–6. [\[CrossRef\]](#)
49. Abdeen, E.; Gaafar, M.A.; Orabi, M.; Wang, F. Predictive Control of Multi-Level Single Phase Microinverter. In Proceedings of the 2019 IEEE International Symposium on Predictive Control of Electrical Drives and Power Electronics (PRECEDE), Quanzhou, China, 31 May–2 June 2019; pp. 1–5. [\[CrossRef\]](#)
50. Abdeen, E.; Gaafar, M.A.; Orabi, M.; Youssef, M. A Novel High Gain Single-phase Transformer-less Multi-level Microinverter. In Proceedings of the 2019 IEEE Applied Power Electronics Conference and Exposition (APEC), Anaheim, CA, USA, 17–21 March 2019; pp. 3263–3268. [\[CrossRef\]](#)
51. Lopez, D.; Flores-Bahamonde, F.; Kouro, S.; Perez, M.A.; Llor, A.; Martínez-Salamero, L. Predictive control of a single-stage boost DC-AC photovoltaic microinverter. In Proceedings of the IECON 2016–42nd Annual Conference of the IEEE Industrial Electronics Society, Florence, Italy, 23–26 October 2016; pp. 6746–6751. [\[CrossRef\]](#)
52. Bahraini, F.; Abrishamifar, A.; Rahmati, A. A Single-Phase Grid-Connected PV Microinverter With Very Low DC Bus Capacitance, Low THD, and Improved Transient Response. In Proceedings of the 2019 10th International Power Electronics, Drive Systems and Technologies Conference (PEDSTC), Shiraz, Iran, 12–14 February 2019; pp. 481–486. [\[CrossRef\]](#)
53. Wan, C.; Li, L.; Wang, C. Adaptive reverse current control and voltage equalization strategy for T-type BCM Microinverter. In Proceedings of the IECON 2020 The 46th Annual Conference of the IEEE Industrial Electronics Society, Singapore, 18–21 October 2020; pp. 1217–1222. [\[CrossRef\]](#)
54. Prabhu, N.S.; Viswadev, R.; Venkatesaperumal, B.; Mishra, S. A Transformerless Photovoltaic Microinverter using High-gain Z-Source Boost Converter for Single-phase Grid connected Applications. In Proceedings of the 2020 IEEE International Conference on Power Electronics, Smart Grid and Renewable Energy (PESGRE2020), Cochin, India, 2–4 January 2020; pp. 1–6. [\[CrossRef\]](#)
55. Zhao, X.; Zhang, L.; Ma, Q.; Lai, J.S. Modeling and control of a wide-input hybrid resonant microconverter for photovoltaic applications. In Proceedings of the 2016 Asian Conference on Energy, Power and Transportation Electrification (ACEPT), Singapore, 25–27 October 2016; pp. 1–6. [\[CrossRef\]](#)
56. Lorenzani, E.; Immovilli, F.; Bianchini, C.; Bellini, A. Performance analysis of a modified Current Source Inverter for photovoltaic microinverter applications. In Proceedings of the IECON 2013–39th Annual Conference of the IEEE Industrial Electronics Society, Vienna, Austria, 10–13 November 2013; pp. 1809–1814. [\[CrossRef\]](#)
57. Liu, W.; Yang, L.; Chen, W.; Wang, Y.; Wang, D.; Li, S. Grid current control of flyback type Micro Inverter based on FASVM. In Proceedings of the 2016 35th Chinese Control Conference (CCC), Chengdu, China, 27–29 July 2016; pp. 8716–8720. [\[CrossRef\]](#)
58. Dhivya, R.; Jaiganesh, K.; Duraiswamy, K. Performance analysis of boost half bridge photovoltaic microinverter using RCC variable step size algorithm. In Proceedings of the 2013 International Conference on Renewable Energy and Sustainable Energy (ICRESE), Coimbatore, India, 5–6 December 2013; pp. 75–80. [\[CrossRef\]](#)
59. Zapata, J.W.; Renaudineau, H.; Kouro, S.; Perez, M.A.; Meynard, T.A. Partial power DC-DC converter for photovoltaic microinverters. In Proceedings of the IECON 2016–42nd Annual Conference of the IEEE Industrial Electronics Society, Florence, Italy, 23–26 October 2016; pp. 6740–6745. [\[CrossRef\]](#)
60. Bhattacharya, A.; Paul, A.R.; Chatterjee, K. A Coupled Inductor Based Ćuk Microinverter for Grid Connected Photovoltaic Applications. In Proceedings of the 2020 IEEE International Conference on Power Electronics, Drives and Energy Systems (PEDES), Jaipur, India, 16–19 December 2020; pp. 1–6. [\[CrossRef\]](#)
61. Xingkui, M.; Qisheng, H.; Qingbo, K.; Yudi, X.; Zhe, Z.; Andersen, M.A.E. Grid-connected photovoltaic micro-inverter with new hybrid control LLC resonant converter. In Proceedings of the IECON 2016–42nd Annual Conference of the IEEE Industrial Electronics Society, Florence, Italy, 23–26 October 2016; pp. 2319–2324. [\[CrossRef\]](#)
62. Chakraborty, S.; Chattopadhyay, S. A Dual-Active-Bridge-Based Fully ZVS HF-Isolated Inverter With Low Decoupling Capacitance. *IEEE Trans. Power Electron.* **2020**, *35*, 2615–2628. [\[CrossRef\]](#)
63. Korosec, L.; Konjedic, T.; Truntic, M.; Rodic, M.; Milanovic, M. Field programmable gate array-based control method for a pulse density modulated microinverter operating in island mode. *IET Power Electron.* **2016**, *9*, 2621–2630. [\[CrossRef\]](#)

64. Dong, D.; Agamy, M.S.; Harfman-Todorovic, M.; Liu, X.; Garcés, L.; Zhou, R.; Cioffi, P. A PV Residential Microinverter With Grid-Support Function: Design, Implementation, and Field Testing. *IEEE Trans. Ind. Appl.* **2018**, *54*, 469–481. [[CrossRef](#)]
65. Zhang, L.; Sun, K.; Li, Y.W.; Lu, X.; Zhao, J. A Distributed Power Control of Series-Connected Module-Integrated Inverters for PV Grid-Tied Applications. *IEEE Trans. Power Electron.* **2018**, *33*, 7698–7707. [[CrossRef](#)]
66. Feng, J.; Wang, H.; Xu, J.; Su, M.; Gui, W.; Li, X. A Three-Phase Grid-Connected Microinverter for AC Photovoltaic Module Applications. *IEEE Trans. Power Electron.* **2018**, *33*, 7721–7732. [[CrossRef](#)]
67. Burbano-Benavides, D.S.; Ortiz-Sotelo, O.D.; Revelo-Fuelagán, J.; Candelo-Becerra, J.E. Design of an On-Grid Microinverter Control Technique for Managing Active and Reactive Power in a Microgrid. *Appl. Sci.* **2021**, *11*, 4765. [[CrossRef](#)]
68. Min, G.H.; Lee, K.H.; Ha, J.I.; Kim, M.H. Design and Control of Single-Phase Grid-Connected Photovoltaic Microinverter with Reactive Power Support Capability. In Proceedings of the 2018 International Power Electronics Conference (IPEC-Niigata 2018-ECCE Asia), Niigata, Japan, 20–24 May 2018; pp. 2500–2504. [[CrossRef](#)]
69. Jain, S.; Easley, M.; Shadmand, M.B.; Mirafzal, B. Decoupled active and reactive power predictive control of impedance source microinverter with LVRT capability. In Proceedings of the 2018 IEEE Power and Energy Conference at Illinois (PECI), Champaign, IL, USA, 22–23 February 2018; pp. 1–6. [[CrossRef](#)]
70. Poshtkouhi, S.; Trescases, O. Flyback Mode for Improved Low-Power Efficiency in the Dual-Active-Bridge Converter for Bidirectional PV Microinverters With Integrated Storage. *IEEE Trans. Ind. Appl.* **2015**, *51*, 3316–3324. [[CrossRef](#)]
71. Barros, L.A.M.; Tanta, M.; Sousa, T.J.C.; Afonso, J.L.; Pinto, J.G. New Multifunctional Isolated Microinverter with Integrated Energy Storage System for PV Applications. *Energies* **2020**, *13*, 4016. [[CrossRef](#)]
72. Chakraborty, S.; Chattopadhyay, S. A multi-port, isolated PV microinverter with low decoupling capacitance and integrated battery charger. In Proceedings of the 2016 IEEE Energy Conversion Congress and Exposition (ECCE), Milwaukee, WI, USA, 18–22 September 2016; pp. 1–8. [[CrossRef](#)]
73. Chiang, H.; Lin, F.; Chang, J. Novel Control Method for Multimodule PV Microinverter With Multiple Functions. *IEEE Trans. Power Electron.* **2018**, *33*, 5869–5879. [[CrossRef](#)]
74. Trujillo Rodriguez, C.; Velasco de la Fuente, D.; Garcera, G.; Figueres, E.; Guacaneme Moreno, J.A. Reconfigurable Control Scheme for a PV Microinverter Working in Both Grid-Connected and Island Modes. *IEEE Trans. Ind. Electron.* **2013**, *60*, 1582–1595. [[CrossRef](#)]
75. Trujillo, C.L.; Velasco, D.; Figueres, E.; Garcera, G.; Ortega, R. Modeling and control of a push-pull converter for photovoltaic microinverters operating in island mode. *Appl. Energy* **2011**, *88*, 2824–2834. [[CrossRef](#)]
76. Trujillo, C.L.; Velasco, D.; Garcera, G.; Figueres, E.; Ortega, R. Reconfigurable control scheme for a microinverter working in both grid connected and island mode. In Proceedings of the 2011 IEEE International Symposium on Industrial Electronics, Gdansk, Poland, 27–30 June 2011; pp. 1477–1481. [[CrossRef](#)]
77. Vera, F.A.M.; Prado, J.D.P.; Moriano, J.J.S.; Zuñiga, C.G.P.; Sal y Rosas Celi, D.E. Bidirectional multiport microinverter and grid-multimode-operation control for a non-linear load. In Proceedings of the 2017 IEEE Workshop on Power Electronics and Power Quality Applications (PEPQA), Bogota, Colombia, 31 May–2 June 2017; pp. 1–6. [[CrossRef](#)]
78. Ji, F.; Mu, L.; Zhu, G. A novel Multi-functional photovoltaic Micro-inverter and its control strategy. In Proceedings of the 2016 IEEE 8th International Power Electronics and Motion Control Conference (IPEMC-ECCE Asia), Hefei, China, 22–26 May 2016; pp. 1302–1305. [[CrossRef](#)]
79. Felgemacher, C.; Jaeger, P.; Kobeissi, A.; Pfeiffer, J.; Wiegand, D.; Kruschel, W.; Dombert, B.; Vasconcelos Araujo, S.; Zacharias, P. Design of Photovoltaic Microinverter for Off-Grid and Grid-Parallel Applications. In Proceedings of the CIPS 2014 8th International Conference on Integrated Power Electronics Systems, Nuremberg, Germany, 25–27 February 2014; pp. 1–6.
80. Zhang, Y.; Yin, Z.; Li, W.; Liu, J.; Zhang, Y. Adaptive Sliding-Mode-Based Speed Control in Finite Control Set Model Predictive Torque Control for Induction Motors. *IEEE Trans. Power Electron.* **2021**, *36*, 8076–8087. [[CrossRef](#)]
81. Parvez, M.; Elias, M.F.M.; Rahim, N.A.; Blaabjerg, F.; Abbott, D.; Al-Sarawi, S.F. Comparative Study of Discrete PI and PR Controls for Single-Phase UPS Inverter. *IEEE Access* **2020**, *8*, 45584–45595. [[CrossRef](#)]
82. Kouros, S.; Perez, M.A.; Rodriguez, J.; Llor, A.M.; Young, H.A. Model Predictive Control: MPC's Role in the Evolution of Power Electronics. *IEEE Ind. Electron. Mag.* **2015**, *9*, 8–21. [[CrossRef](#)]
83. Khazaei, J.; Tu, Z.; Asrari, A.; Liu, W. Feedback Linearization Control of Converters With LCL Filter for Weak AC Grid Integration. *IEEE Trans. Power Syst.* **2021**, *36*, 3740–3750. [[CrossRef](#)]
84. Hannan, M.A.; Ghani, Z.A.; Hoque, M.M.; Ker, P.J.; Hussain, A.; Mohamed, A. Fuzzy Logic Inverter Controller in Photovoltaic Applications: Issues and Recommendations. *IEEE Access* **2019**, *7*, 24934–24955. [[CrossRef](#)]